

Research Articles: Systems/Circuits

Double cones and the diverse connectivity of photoreceptors and bipolar cells in an avian retina

<https://doi.org/10.1523/JNEUROSCI.2495-20.2021>

Cite as: J. Neurosci 2021; 10.1523/JNEUROSCI.2495-20.2021

Received: 23 September 2020

Revised: 3 March 2021

Accepted: 1 April 2021

This Early Release article has been peer-reviewed and accepted, but has not been through the composition and copyediting processes. The final version may differ slightly in style or formatting and will contain links to any extended data.

Alerts: Sign up at www.jneurosci.org/alerts to receive customized email alerts when the fully formatted version of this article is published.

1 **Double cones and the diverse connectivity of photoreceptors and bipolar cells in an**
2 **avian retina**

3
4 **Avian double cone and bipolar cell connectivity**

5

6 Anja Günther¹, Karin Dedek¹, Silke Haverkamp², Stephan Irsen², Kevin L. Briggman², Henrik

7 Mouritsen^{1,3,4*}

8 **Affiliations:**

9 ¹ Institute for Biology and Environmental Sciences, Carl von Ossietzky University of Oldenburg, Carl-
10 von-Ossietzky-Straße 9-11, 26129 Oldenburg, Germany

11 ² Center of Advanced European Studies and Research (caesar), Ludwig-Erhard-Allee 2, 53175 Bonn,
12 Germany

13 ³ Research Centre for Neurosensory Sciences, Carl von Ossietzky University of Oldenburg, Carl-von-
14 Ossietzky-Straße 9-11, 26129 Oldenburg, Germany

15 ⁴ Lead contact

16 *Correspondence: henrik.mouritsen@uni-oldenburg.de

17 **Number of pages:** 49; **Number of main figures:** 6

18 **Extended Data:** Figures: 21, tables: 4

19 **Words:** Abstract: 199, Introduction: 654, Discussion: 1620

20 **Conflict of interest:** The authors declare no competing financial interest.

21 **Acknowledgement:** We are grateful to Pranav Seth for volunteering to help grouping the bipolar cells.

22 We are also grateful to Kara Fulton and Timothy Lee for their support in performing additional analyses

23 using MATLAB. This project was funded by the Air Force Office of Scientific Research (Air Force Materiel

24 Command USAF award FA9550-14-1-0095) to H.M., by the Deutsche Forschungsgemeinschaft

25 (SFB1372: Navigation and Magnetoreception in Vertebrates, project number: 395940726 and DFG

26 research training group grant GRK 1885; both to H.M. and K.D.). H.M. also acknowledges funding from

27 the European Research Council (under the European Union's Horizon 2020 research and innovation

28 programme, grant agreement no. 810002 (Synergy Grant: “QuantumBirds”). In addition, funding was
29 provided by Stiftung Caesar (S.H., S.I., and K.L.B.).

30 **Abstract**

31 Double cones are the most common photoreceptor cell type in most avian retinas, but their precise
32 functions remain a mystery. Among their suggested functions are luminance detection, polarized light
33 detection, and light-dependent, radical-pair-based magnetoreception. To better understand the
34 function of double cones, it will be crucial to know how they are connected to the neural network in
35 the avian retina. Here we use serial sectioning, multi-beam scanning electron microscopy (ssmSEM) to
36 investigate double cone anatomy and connectivity with a particular focus on their contacts to other
37 photoreceptor and bipolar cells in the chicken retina. We found that double cones are highly connected
38 with neighbouring double cones and with other photoreceptor cells through telodendria-to-terminal
39 and telodendria-to-telodendria contacts. We also identified 15 bipolar cell types based on their axonal
40 stratifications, photoreceptor contact pattern, soma position, and dendritic and axonal field mosaics.
41 Thirteen of these 15 bipolar cell types contacted at least one or both members of the double cone. All
42 bipolar cells were bi- or multistratified. We also identified surprising contacts between other cone
43 types and between rods and cones. Our data indicate a much more complex connectivity network in
44 the outer plexiform layer of the avian retina than originally expected.

45

46 **Significance statement**

47 Like in humans, vision is one of the most important senses for birds. Here, we present the first serial
48 section multi-beam scanning electron microscopy dataset from any bird retina. We identified many
49 previously undescribed rod-to-cone and cone-to-cone connections. Surprisingly, of the 15 bipolar cell
50 types we identified, 11 received input from rods and 13 of 15 received at least part of their input from
51 double cones. Therefore, double cones seem to play many different and important roles in avian retinal
52 processing, and the neural network and thus information processing in the outer retina is much more
53 complex than previously expected. These fundamental findings will be very important for several fields
54 of science, including vertebrate vision, avian magnetoreception, and comparative neuroanatomy.

55 **Introduction**

56 The visual system of birds is one of the most complex among vertebrates and its importance for birds
57 is reflected by the size of their eyes occupying up to 50% of the cranial volume (Waldvogel, 1990), their
58 large number of retinal neurons (Seifert et al., 2020) and the presence of one or two foveas and/or a
59 visual streak in the retina of many avian species (Wood, 1917). It is thus surprising that little is known
60 about the anatomical ultrastructure and the connectivity of avian retinal cells.

61 Beside rods, birds have four types of single cones enabling tetrachromatic vision (Hart, 2001).
62 Additionally, birds have double cones which often make up 40% of the cone population in the retina.
63 Double cones are common among vertebrates except for eutherian mammals, elasmobranches and
64 catfish (Walls, 1942; Ebrey and Koutalos, 2001). In contrast to some fish double cones, both members
65 of bird double cones contain the same long wavelength sensitive opsin (LWS) (Hart, 2001). The
66 principal member contains one oil droplet whereas the accessory member can have several oil droplets
67 which can differ in size and number (Pedler and Boyle, 1969). In general, oil droplets act as long-pass
68 filters and can have different absorption properties (Stavenga and Wilts, 2014).

69 The function of double cones is still debated (Seifert et al., 2020) and may differ between vertebrate
70 classes. In fish, double cones have been implicated in colour vision due to different opsins in the
71 individual double cone members (Ebrey and Koutalos, 2001). Additionally, they might be involved in
72 polarisation vision since they form mosaics with neighbouring double cones being oriented 90° to each
73 other (Horváth, 2014). Double cones in birds could play a role in movement detection, because the
74 spectral sensitivity of motion-sensitive cells is comparable to the spectral sensitivity of birds' LWS
75 pigments expressed in double cones and long wavelength single cones (Jones and Osorio, 2004; Osorio
76 and Vorobyev, 2005). Furthermore, behavioural conditioning experiments link double cones to
77 mediating fine pattern recognition (Lind and Kelber, 2011).

78 Additionally, double cones were suggested to be involved in light-dependent, radical-pair-based
79 magnetoreception (Zapka et al., 2009; Hore and Mouritsen, 2016; Günther et al., 2018) which is

80 important for orientation and navigation (Wiltschko and Wiltschko, 1995; Kishkinev et al., 2015;
81 Chernetsov et al., 2017; Mouritsen, 2018). Double cones of several bird species including chicken
82 express cryptochrome 4 (Günther et al., 2018) which could be the primary magnetic sensory molecule
83 as it binds the crucial FAD co-factor (Hore and Mouritsen, 2016; Zoltowski et al., 2019). Double cones
84 could be suitable locations for magnetoreceptive molecules since light intensity and polarization
85 information could be separated from the magnetic field information by having two sensors oriented
86 differently in each member of double cones (Worster et al., 2017).

87 Fundamental anatomical insights into pigeon photoreceptors were provided by Mariani and Leure-du
88 Pree (1978) showing e.g. that rods and double cones stratify in the first (outermost) stratum of the tri-
89 stratified outer plexiform layer (OPL) which was also found in chicken (Tanabe et al., 2006).
90 Furthermore, electron microscopic data from chick retina suggest a coupling of both members of a
91 double cone through junction-like structures (Nishimura et al., 1981). However, a systematic structural
92 analysis of double cones is missing. Two studies identified bipolar cell types in the chicken (Quesada et
93 al., 1988) and pigeon retina (Mariani, 1987). Although these studies provide important knowledge
94 about photoreceptors and bipolar cells in the avian retina, information on potential
95 photoreceptor/photoreceptor and bipolar cell/photoreceptor connections are lacking.

96 Since these classic electron microscopic studies, electron microscopic techniques underwent a
97 constant development (for review see Peddie and Collinson, 2014). By using a new development,
98 namely serial sectioning multi-beam scanning electron microscopy (ssmSEM) (Eberle and Zeidler,
99 2018), the aim of the present study was to provide a detailed analysis of the double cones' anatomy
100 and their connections to other photoreceptor and bipolar cell types. Furthermore, we reconstructed
101 74 complete bipolar cells through which an extended bipolar cell type classification emerged.

102

103 **Materials and Methods**

104 **Animals**

105 One-week old domestic chickens (*Gallus gallus domesticus*) were hatched in the teaching and research
106 station Frankenforst (Königswinter, Germany). All animal procedures were approved by the Animal
107 Care and Use Committees of the Niedersächsisches Landesamt für Verbraucherschutz und
108 Lebensmittelsicherheit (LAVES, Oldenburg, Germany) and the Landesamt für Natur, Umwelt und
109 Verbraucherschutz Nordrhein-Westfalen (LANUV, Recklinghausen, Germany). The age of an
110 experimental animal may have a crucial influence on the morphology and connectivity of the analyzed
111 cells. However, retinal cell type differentiation and synaptogenesis in the plexiform layers in chicken
112 already starts at an embryonic stage (Drenhaus et al., 2003, 2007), and major receptor types can
113 already be detected at E12 (Hering and Kröger, 1996), for review see (Mey and Thanos, 2000).
114 Therefore, the cell development in our one-week old chicken is completed and the synaptogenesis is
115 advanced, but it is unclear whether it is entirely completed.

116 **Sample preparation for electron microscopic recordings**

117 Birds were killed by decapitation and eyes were removed immediately. Lens apparatus and vitreous
118 body were removed, and eyecups were fixed in a 0.08 M cacodylate (Sigma Aldrich, St Louis, USA)
119 buffer (pH=7.4) containing 2.5% paraformaldehyde (Carl Roth, Karlsruhe, Germany) and 1.25%
120 glutaraldehyde (EMS Hatfield, USA) for 30 minutes at room temperature. Retinas were removed from
121 the eyecup and transferred into a 0.08 M cacodylate buffer (pH=7.4) two times for 15 minutes each.

122 Basic staining procedure was performed after Hua et al. 2015. Before embedding, the tissue was
123 dehydrated through a graded ethanol series (50%, 75%, 100%, 30 minutes each at 4 °C), followed by
124 washing three times in 100% anhydrous acetone (VWR, Radnor, USA) at room temperature for 30
125 minutes each. For epon infiltration, the tissue was first incubated in 1:2 mixture of anhydrous acetone
126 and Embed812 resin hard formulation (20 ml Embed812, 9 ml DDSA, 12 ml NMA and 0.72 ml DMP-30;
127 EMS) over night at room temperature followed by 8 h incubation in pure Embed812 resin at room
128 temperature. Retinas were cut into smaller pieces and position within the retina was mapped before

129 transferring the smaller tissue pieces into embedding moulds (Ted Pella) for polymerisation at 70 °C
130 for 48 h.

131 **Sample sectioning and data acquisition for electron microscopy**

132 After polymerisation, a piece of the dorsal periphery in the left eye was pre-trimmed with a hand saw
133 and afterwards trimmed to a block face of approximately 900 μm x 250 μm using a Leica
134 ultramicrotome UC7. For the 3D reconstruction dataset, serial sectioning of 40 nm thick slices from a
135 sample in the periphery of the left eye of one chicken was performed with a Diatome ultra ats diamond
136 knife with a knife angle of 35° (Science Services, Germany). 271 sections of 900 x 250 μm were collected
137 on a glow discharged silicon wafer (Active Bizz, Germany) and dried on a heating plate at 50 °C until
138 the water was fully evaporated. The wafer was mounted with silver paint (Plano) on a multi Sem
139 Universal holder Version 2 and stored in a heated vacuum chamber until further use. An overview
140 image from the complete wafer was recorded with a Zeiss Axio Imager.A2 Vario. Individual slices were
141 marked and tracked using Zen2 (blue edition) (Zeiss). The chicken sample was recorded with a 91-
142 parallel-beam Zeiss MultiSEM 506, where the parallel beams are hexagonally arranged to decrease
143 electron-optical aberrations (Eberle et al., 2015). Recordings were performed with a beam current of
144 591 pA, landing energy of 1.5 keV, 400 ns pixel dwell time per beam and a pixel size of 4 nm. A volume
145 area of approximately $9 \times 10^3 \mu\text{m}^3$ was imaged, resulting in 11,985 hexagonally shaped multi-beam
146 fields of view (mFOV), containing more than one million high-resolution images and about 1.36×10^{10}
147 megapixels. Hexagonal mFOVs consisted of 91 rectangular, single-beam image tiles with a tile size of
148 3,800 x 3,292 pixels for each tile. Tile overlap was 500 nm and mFOV overlap was 8%. Single-beam
149 images were stored as TIF-files accumulating 14.3 TB of storage space. To correct for scan distortion,
150 a built-in algorithm was used. 2D alignment of all tiles per region was also performed by a built-in
151 algorithm. One retinal slide consisting of several mFOVs is further on named region. In total, 271
152 sections were recorded.

153 For detailed 2D analysis of double cone morphological structures, 40 nm thick sections of nine chicken
154 were cut with an ultra 35° diamond knife (Diatome) and transferred on carbon coated copper grids

155 with a hole size of 35/10 nm (S35/10, Quantifoil, Großlöbichau, Germany). Images were recorded with
156 a Jeol JEM-2200FS at an energy of 200 keV with a TEM-CAM F416 cmos camera (TVIPS) at a
157 magnification of 40,000x resulting in a pixel size of 0.322 nm.

158 **Image processing and reconstruction of electron microscopic serial sections**

159 Due to the tile overlap of 500 nm of the mFOVs, the overlapping part of the image was exposed twice
160 to an electron beam which caused higher bleaching than in the rest of the image. To correct for these
161 differences in brightness, a self-written script containing a bandpass filter was applied on every single
162 tile. Image processing was performed using the plugin TrakEM2 from the Fiji package (Schindelin et al.,
163 2012). All single tiles from one region were loaded into TrakEM2 using the provided text file with
164 individual tile coordinates. To decrease the size of the dataset and increase processing speed, the
165 dataset was divided into seven sub-volumes. For each sub-volume, a single image per slice was created.
166 Single images were afterwards merged into one 3D dataset using the tif2mrc program from the imod
167 package (Kremer et al. 1996). For 3D alignment of the individual slides in the sub-volumes we used the
168 MIDAS program from imod. For the 3D volume reconstruction of one individual double cone, the
169 alignment of a smaller sub-volume reaching from the pigment epithelium to the beginning of the inner
170 nuclear layer (INL) and a size of $47.7 \mu\text{m} \times 75.6 \mu\text{m} \times 10.4 \mu\text{m}$ was refined using MIDAS. Due to memory
171 limitation on the computer, we created a volume of $140 \mu\text{m} \times 148 \mu\text{m} \times 10.4 \mu\text{m}$ size reaching from
172 the outer nuclear layer (OPL) to the ganglion cell layer (GCL) to reconstruct complete bipolar cells and
173 photoreceptor cells. For all 3D volume reconstructions of individual cells, the 3dmod program from
174 imod was used (see Fig. 1-1F for the two sub-volumes analyzed).

175 **Analysis of photoreceptor cells and bipolar cells in a 3D volume**

176 To calculate the ratio of the different photoreceptor cell types, photoreceptors of the complete data
177 set were analyzed. Only photoreceptor cells which could be clearly identified as one specific type of
178 photoreceptor went into the statistical analysis. Based on the stratification level in the OPL, long
179 wavelength single cones (red cones) and middle wavelength single cones (green cones) could not be

180 distinguished and were sampled in one group. Likewise, short wavelength single cones (blue cones)
181 and ultra-short wavelength single cones (violet cones) could not be distinguished and were also
182 sampled in one group. To further analyse the structure and connectivity strength of the cells' terminals,
183 we counted all the ribbon synapses present in twenty terminals of rods, single cones, and double
184 cones. Afterwards, the mean and standard deviation was calculated. Telodendria or bipolar cell
185 dendrites that reached into the terminal of a photoreceptor and ended there with contacting the
186 terminal other than at a ribbon synapse were classified as "basal contact". Telodendria or bipolar cell
187 dendrites that reached into the terminal of a photoreceptor and ended without making a contact were
188 classified as "no clear contact". If a bipolar cell dendrite or photoreceptor telodendrion contacted a
189 terminal from a photoreceptor but did not end there, it was also classified as "no clear contact". For
190 evaluating the dendritic and axonal fields of the bipolar cells, we drew the convex hull for each axon
191 terminal and dendritic field. Classification of bipolar cell types was performed blindly by four untrained
192 researchers to avoid bias. Connectivity matrices were calculated based on the normalized number of
193 basal or ribbon synapses, respectively, using MATLAB (Higham and Higham, 2016). Pre- and
194 postsynaptic distributions from basal and ribbon contacts were calculated as followed: For the
195 presynaptic distribution of basal contacts, we counted the basal contacts (Fig. 3-2 triangles) within the
196 terminal of one photoreceptor cell type to a specific postsynaptic cell (Fig. 3-2A, e.g., bright blue for
197 AC) and divided it by the number of all the detected basal contacts in the terminals (Fig. 3-2A, all
198 triangles). The same procedure was performed for the presynaptic distribution of ribbon contacts,
199 where we divided the number of ribbon contacts from one cell type by the number of all ribbon
200 synapses identified within the terminal. For the postsynaptic distribution of synapses, we also counted
201 all the basal and ribbon contacts that a postsynaptic cell type made within the terminal of a specific
202 photoreceptor cell type (Fig. 3-2A, triangles or squares in bright blue for AC) and divided it by the total
203 number of basal or ribbon synaptic contacts that photoreceptor cell type made (not shown in the
204 figure).

205 Basal contacts were divided into three classes based on their distance to the nearest ribbon synaptic
206 contact: triad associated, middle non-triad associated, and marginal non-triad associated (Fig. 4-1 to
207 Fig. 4-15). Basal contacts were classified as middle non-triad associated if at least two dendrites
208 separated this dendrites from the nearest ribbon synapse and as marginal non-triad associated if they
209 contacted the terminal at the outer margin or at elongations of the terminal other than telodendria
210 (see Tsukamoto and Omi, 2015).

211 The stratification profiles in Fig. 5 for each bipolar cell type were calculated as probability density
212 function estimates, using the scatterhist function in MATLAB after calculating the mean cell volume of
213 each bipolar cell type for each drawn contour. In Fig. 4-1 to Fig. 4-15 panel B the sum of each cell
214 volume along the y-axis was calculated and overlaid with the total sum of all cells within the volume
215 (black line).

216 **Immunohistochemistry**

217 For immunohistochemical analysis, eyecups from four one-week old chicken were prepared by cornea
218 dissection followed by removal of the lens and vitreous body. Eyecups were fixed in 4% PFA/PBS for
219 30 min and afterwards washed three times for 10 min in PBS. Part of the retina was removed from the
220 eyecup as stripes (width ~4 mm), reaching from the dorsal periphery to the centre tip of the pecten.
221 The retinal stripes were afterwards embedded in 4% high-melting agarose. for vibratome sections, 100
222 μ m thick vibratome sections were collected and triple staining using GNB3 antibody (CatNo. LS-B8347,
223 Lifespan Biosciences, USA), diluted 1:200, PKC alpha clone MC5 (CatNo. K01107M, Biodesign
224 International, USA), diluted 1:100, and Ctbp2 (CatNo. 193003, Synaptic Systems, Germany), diluted
225 1:5000 in PBS including 1% TritonX-100 and 3% normal donkey serum, was performed overnight at
226 room temperature. At the next day, retina slices were washed four times 10 minutes in PBS and GNB3
227 visualization was performed using Alexa 488, Cy3 and Alexa 647-conjugated secondary antibodies
228 (Dianova, Germany) 1:500, in PBS including 1% Triton and 3% normal donkey serum for two hours at
229 room temperature. In addition to the secondary antibodies, we included DAPI (Sigma Aldrich, USA;
230 1:10.000) to stain cell nuclei. Retinal slices were again washed four times 10 minutes, mounted on

231 slides and covered with Aqua-Poly/Mount (Polysciences, Germany) and a coverslip. Confocal
232 micrographs of fluorescent retinas were analyzed with a TCS SP8 confocal microscope (Leica Camera
233 AG, Wetzlar, Germany) using the 405 nm and 488 nm lines and the PMT settings were chosen to avoid
234 cross-talk between the different lines. Scanning was performed with the glycine immersion HC PL APO
235 63x / 1.30 GLYC CORR CS2 at a resolution of 2,048 x 2,048 pixels. Stacks were recorded with a thickness
236 of 12 μm and final images were z-projections of the complete stack adjusted in brightness and contrast
237 in ImageJ (NIH, Bethesda, MD, USA).

238 **Results**

239 **Identification of different photoreceptor types**

240 We used the novel ssmSEM technique to acquire a high-resolution 3D electron microscopic dataset
241 from a 900 x 250 x 10.4 micrometre area in the dorsal periphery of the left retina of a one-week-old
242 chicken to analyse the morphology of double cones in 3D and gain insights into their connections to
243 bipolar cells and other photoreceptor cells. For a first estimation, we identified all the photoreceptor
244 cell types in the complete dataset using already described morphological features, such as the
245 presence of an oil droplet in all cones (Bowmaker, 2008), location of the cell bodies of photoreceptor
246 cells in the outer nuclear layer (ONL), the ending of the synaptic terminals in the three strata of the
247 OPL (Mariani and Leure-du Pree, 1978; Mariani, 1987), and glycogen accumulations in the inner
248 segments of rods (hyperboloid) and the accessory member of the double cones (paraboloid) (Meyer
249 and May, 1973). As the green and red single cones both have their synaptic terminals located in the
250 second strata and the blue and violet single cones both have their synaptic terminals located in the
251 third strata in the OPL (Mariani and Leure-du Pree, 1978), we were not able to differentiate between
252 the two cell types of each pair and therefore grouped them together as green/red (G/R) and blue/violet
253 cones (B/V). In total, 706 photoreceptor cells were counted. 228 of these were identified as double
254 cones, 130 as combined green (medium-wavelength sensitive, MWS) or red (long-wavelength
255 sensitive, LWS) single cones, 51 as blue (short-wavelength sensitive, SWS2) or violet (short-wavelength

256 sensitive, SWS1) single cones, and 244 as rods. We were able to identify 53 additional photoreceptors
257 as single cones, but we could not characterise them further because essential morphological features
258 were missing, e.g., the terminal within the OPL. In summary, we found 32.3% double cones, 34.6% rods
259 and 33.1% single cones. Thus, 49.4% of all cones were double cones.

260 In the process of collecting serial sections, some slices were lost, leading to a ~160 nm gap (marked
261 with a black line in Fig. 1A) in the 140 μm x 148 μm x 10.4 μm sub-volume. Despite this gap, we were
262 still able to track most of the processes from photoreceptors as well as the dendrites and axons from
263 bipolar cells (Fig. 1B, Fig. 1-1).

264 The terminals of the rods and both members of double cones form a mosaic (Fig. 1C, 1D) as do the
265 terminals from the green/red cones (Fig. 1E, green). The terminals of the blue/violet cones seem to
266 cluster together (Fig. 1E, magenta). The photoreceptor terminals from rods and double cones can be
267 found in stratum 1 of the OPL whereas the terminals from G/R single cones are located in the second
268 stratum and the terminals from B/V single cones in the third stratum (Fig. 1F).

269 **Morphological characterisation of the double cone**

270 With the high-resolution 3D reconstruction of a complete double cone, including all its major
271 compartments, we reinvestigated the double cone anatomy in the chicken retina (Fig. 2A, sub-volume
272 1, Fig. 1-1F). We could identify multiple tiny oil droplets in the accessory member of the double cone
273 and a single oil droplet in the principal member as indicated by Pedler and Boyle (1969). Due to the
274 small size of the multiple oil droplets in the accessory member, they may have been overlooked in light
275 microscopic studies (López-López et al. 2008) leading to different opinions on whether or not the
276 accessory member of double cones has a fractionated oil droplet. The principal member has a mean
277 number of 9.1 ± 3.2 ($n=14$, mean \pm SD) processes, which spread radially but never exceed the first
278 stratum of the OPL. In contrast, the accessory member extends several short processes towards the
279 principal member and additionally 2.8 ± 0.7 ($n=14$) long processes, which pass underneath the terminal

280 of the principal member and can reach the third stratum of the OPL (Fig. 2A). Processes were only
281 analyzed from double cone members where the complete terminal was in the volume.

282 For an even more detailed view on specific structures in the double cone, we used transmission
283 electron microscopy. By analysing the highly stacked and ordered membranes in the outer segments
284 of the double cone, we validated the tissue preservation (Fig. 2B) and were able to visualize the outer
285 membrane invaginations (Fig. 2C). A closer look into the opposing membranes of the double cone
286 members confirmed junction-like structures along the inner segments of the double cones (Fig. 2D),
287 which may represent gap junctions as described by Nishimura and colleges (Nishimura et al., 1981).
288 Additionally, we observed that only the accessory member of the double cone expressed a paraboloid
289 which is a region of accumulated glycogen surrounded by a large density of endoplasmic reticuli
290 (Cohen, 1972). However, we did not find any specialized structure that could have evolved specifically
291 for the putative functions of chicken double cones in magnetoreception and/or polarized light vision.

292 **Classification of photoreceptor contacts**

293 Having confirmed the morphology of double cones in chicken, we investigated how double cones are
294 connected to other photoreceptors and how the photoreceptors are connected to bipolar cell types.
295 To characterize connecting cells, we first determined what is an actual contact and which type of
296 contact cells make with each other. However, the typical morphology of ribbon synapses (Meller, 1964;
297 Dowling and Boycott, 1966; Lagnado and Schmitz, 2015) and basal (flat) contacts (Dowling and Boycott,
298 1966; Haverkamp et al., 2000) in the photoreceptor terminals could still be identified and were used
299 to classify the type of contact (for details, see method section). Ribbon synapses are located inside the
300 photoreceptor terminal (Fig. 2E). Two lateral horizontal cell dendrites and one or two central bipolar
301 cell dendrites invaginate the photoreceptor terminal at sites where ribbons are anchored (Dowling and
302 Boycott, 1966). In general, ON bipolar cells usually make invaginating (central) contacts, OFF bipolar
303 cells usually make basal (flat) contacts at the base of the photoreceptor terminal (Haverkamp et al.,
304 2000). But there are several exceptions, where OFF bipolar cells occupy the central part of a ribbon
305 synapse (fish: Saito et al., 1985 or ON bipolar cells make basal contacts Calkins et al., 1996). In the

306 turtle, the lateral or central positions could also be occupied by a process from another photoreceptor
307 (Mariani and Lasansky, 1984).

308 **The number of ribbon synapses**

309 We first counted the number of ribbon synapses expressed in a subset of rod and cone terminals. Since
310 the terminals of green and red cones as well as blue and violet cones terminate in the second and third
311 strata of the OPL, respectively, the number of ribbons provided below is the average number for the
312 respective two types combined. In contrast to rodent rods, which only express one ribbon per terminal
313 (Cohen, 1960; Ladman, 1958), rods from chicken contained 3 ± 0.8 ($n=20$) ribbons per terminal. In
314 double cones, the mean number of ribbons was larger in the principal member (18.5 ± 2.0 , $n=20$) than
315 in the smaller accessory member (8.7 ± 0.8 , $n=20$). The terminals of single cones contained a similar
316 number of ribbons (green/red single cones: 9.5 ± 1.4 , $n=20$; blue/violet single cones: 8.9 ± 1.3 , $n=10$).
317 Ribbon synapses were only counted in complete terminals of rods and cones throughout the dataset.

318 **Identification of photoreceptor/photoreceptor connections**

319 Telodendria are present at the photoreceptor terminals of various vertebrate species (e.g. cats (Kolb,
320 1977), primates (O'Brien et al., 2012), zebrafish (Li et al., 2009; Noel and Allison, 2018)), and birds
321 (Mariani and Leure-du Pree, 1978)). While telodendria were shown to be coupled by gap junctions in
322 a number of species [e.g., ground squirrel (DeVries et al., 2002); primate (Hornstein et al., 2005); and
323 zebrafish (Noel and Allison, 2018)], telodendria of turtle photoreceptors invaginate into neighboring
324 terminals, making chemical contacts at the ribbon synapse (Ammermüller and Kolb, 1996; Mariani and
325 Lasansky, 1984; Kolb and Jones, 1985; Owen, 1985).

326 The analysis of photoreceptor/photoreceptor contacts was performed in sub-volume 2 ($140 \mu\text{m} \times 148$
327 $\mu\text{m} \times 10.4 \mu\text{m}$ Fig. 1-1F). By analysing tip-to-tip and tip-to-shaft telodendria contacts (for definition,
328 see Fig. 3-1A, B), which most likely represent gap junctions, we found that tip-to-tip contacts only
329 occurred between cells of the same cell type, predominantly between rods and in smaller numbers
330 also between the principal members of the double cone and green/red single cones (Fig. 3-1C). Tip-to-

331 shaft telodendrial contacts were detected between cells from the same type but also between cells
332 from different photoreceptor cell types with the highest numbers being observed between different
333 single cone types (Fig. 3-1D). Although telodendria are abundant in the chicken OPL, contacts of
334 telodendria-telodendria are rather restricted (18.4% of total number of detected contacts) and most
335 of the photoreceptor telodendria make contact within the terminals of other photoreceptors.

336 However, as in the turtle, chicken photoreceptor telodendria frequently contacted other
337 photoreceptor terminals via basal and ribbon contacts which looked similar to the basal and ribbon
338 contacts between bipolar cells and photoreceptor cells described above. The accessory members of
339 double cones are highly connected with their affiliated principal member by telodendrial basal and
340 ribbon contacts in the terminal of the principal member (Fig. 3B, F-I). In contrast, the principal member
341 is less connected, making only basal contacts with its affiliated accessory member and no ribbon
342 contacts at all (Fig. 3B right, F-I). Principal members also made basal contacts to the terminal of other
343 principal members (Fig. 3A, F-I). In contrast, accessory members from different double cones never
344 made any contacts to each other (Fig. 3F-I).

345 Due to the length of the descending telodendria of the accessory members, we could not identify all
346 contacts because the processes reached the end of the volume. Only in six AC cells we identified either
347 basal or ribbon contacts directly to green/red cone terminals (Fig. 3C, F-I). In one case, we found a long
348 telodendrion of an accessory member making a basal contact to a blue/violet cone (Fig. 3F, G).

349 Reconstructing the group of blue/violet cones, we discovered that these single cones not only have
350 long telodendria at their terminals but also extend shorter telodendria into the first stratum of the
351 OPL. However, some primary telodendria reached the end of the volume and therefore the area in the
352 first stratum could not be completely reconstructed. Nonetheless in three of the cells, we found that
353 these shorter telodendria made basal contacts at the terminal of the principal member of double cones
354 (Fig. 3D, F, G). We found that B/V single cones do not contact each other but rather contact G/R single
355 cones (Fig. 3F-I).

356 Almost all rods (90%) contacted the terminal of principal members of double cones with their
357 telodendria via basal contacts (Fig. 3E, F, G). Although these rods received major input from the
358 principal member, it is interesting to note that these rods were mostly presynaptic to other rods
359 representing an asymmetry in signal transduction.

360 However, immunohistological stainings of connexins, the building blocks of gap junctions, indicated
361 that gap junctions could also be present within the terminals of photoreceptors in the chicken retina
362 (Kihara et al., 2009). Therefore, it could be possible that telodendria and photoreceptor terminals form
363 not only chemical synapses but also gap junctions.

364 In summary, these analyses reveal a surprisingly complex network of connections among bird
365 photoreceptors, suggesting that the bird retina is more similar to other sauropsida retinas such as the
366 turtle (Mariani and Lasansky, 1984) than to the mammalian (Hornstein et al., 2005) or fish retina (Noel
367 and Allison, 2018) in this regard. All individual photoreceptor contacts are listed in figures 3-3 to 3-6.

368 **Identification of bipolar cell types**

369 Since the connectivity between photoreceptors and bipolar cells is unknown for birds and because the
370 number of previously anatomically described bipolar cell types in the bird retina seemed surprisingly
371 low (11 in chicken, 8 in pigeon) (Mariani, 1987; Quesada et al., 1988), in sub-volume 2 (Fig. 1-1F), we
372 reconstructed all bipolar cells that contacted at least one of the reconstructed photoreceptors. Bipolar
373 cells which had their main dendritic and axonal fields inside the volume were considered as complete
374 cells (n=74). These cells were used for identifying the connectivity between bipolar cells and
375 photoreceptor cells and for defining bipolar cell types. Bipolar cells, of which the primary axon reached
376 the end of the volume or major parts of the dendritic field were missing, were defined as partial bipolar
377 cells (n=72) and were only further analyzed if they could be clearly assigned to one bipolar cell type
378 (e.g., based on contacted photoreceptor types, fitting into the existing dendritic mosaic). Dendrites
379 that contacted photoreceptors but were not connected to a soma were ignored. In order to identify
380 the stratification level of the axons in the inner plexiform layer (IPL), we chose to divide the IPL in eight

381 strata based on an earlier study analysing the stratification of ganglion cells in chicken retina (Naito
382 and Chen, 2004).

383 With the dataset at hand, we not only analyzed the morphology (dendritic and axonal stratification,
384 soma position) of the bipolar cells, but also their contacts to the different photoreceptor types to
385 define bipolar cell types. In a final step, we double checked the different types by analysing the
386 dendritic and axonal field mosaics as described for bipolar cells from other species, such as mouse
387 (Wässle et al., 2009; Tsukamoto and Omi, 2017) and primates (Boycott and Wässle, 1991). In total, we
388 identified 15 types of bipolar cells in the chicken retina, sorted by the position of their axonal
389 stratification (Fig. 4 A). Detailed information on each bipolar cell type is given in Fig. 4-1 to Fig. 4-15. In
390 addition, we classified two fully reconstructed bipolar cells as “orphan” because they could not be
391 assigned to any other bipolar cell type and are also different from each other (Fig.4-16).

392 For all bipolar cells, we analyzed the type of contact they made to photoreceptor terminals (ribbon
393 versus basal contacts). We further categorized the basal contacts based on their distance to the
394 nearest ribbon synapse (Fig. 4-1F to Fig. 4-15F). Examples of this analysis are shown in Fig. 4B-G with
395 B2 as a potential ON bipolar cell type, B5a as a potential midget bipolar cell type and B7 as a potential
396 OFF bipolar cell type. We also analyzed whether bipolar cells contacted all the photoreceptors of a
397 specific type within their dendritic field and found that no bipolar cell type seemed to avoid a terminal
398 of a photoreceptor type it normally contacts (Fig.4-1G to 4-15G). We calculated the stratification
399 density probabilities of each individual bipolar cell type based on the calculated volume of the cells
400 along retina depth (Fig. 5) reflecting the overall stratification pattern in the OPL and IPL. To visualize
401 how much volume each bipolar cell contributes to the different strata in the IPL, we calculated the
402 mean volume of all cells from a bipolar cell type along IPL depth (Fig. 4-1B to Fig.4-15B, coloured lines)
403 and calculated the sum of all bipolar cells (Fig.4-1B to Fig.4-15B, black line) which enabled us to identify
404 the overall distribution of bipolar cells along IPL depth. We found that strata 3, 5 and 8 have the lowest
405 density of bipolar cell terminals. However, we cannot exclude that we are missing bipolar cell types
406 because our data set is limited in the z-direction.

407 In the OPL, we found some exclusive connections between bipolar cells and photoreceptors.
408 Surprisingly, only one type (B9) exclusively contacts green/red single cones and one type (B10)
409 exclusively contacts blue/violet cones. B10 bipolar cells may represent the “blue bipolar cell” known
410 from mammalian species [e.g. mouse (Haverkamp et al., 2005), primate (Mariani, 1984; Ghosh et al.,
411 1997) and ground squirrel (Li and DeVries, 2006)], but we would have had to be able to separate blue
412 from violet single cones in the dataset to clearly identify single cone type specific bipolar cells. One
413 type (B6) seems to contact almost exclusively the accessory member of double cones (Fig. 4A and Fig.
414 4-11). All other bipolar cell types (except for B9 and B10) make contacts to several photoreceptor cell
415 types but receive most of their input from the principal member of double cones (Fig. 4-1 to 4-13).
416 Interestingly rods make most of their ribbon synaptic contacts to B2 bipolar cells (Fig. 4-3). Additionally,
417 12 of the 15 identified bipolar cells receive input from rods.

418 **Identification of the ON-OFF border in the IPL**

419 We were able to identify 15 different bipolar cell types including their connectivity to photoreceptor
420 cells. Since electrophysiological data from avian bipolar cells are completely lacking, we aimed to
421 identify a putative border between the OFF and ON strata in the IPL using immunohistochemistry in
422 order to analyse which of the identified cell types may represent ON or OFF bipolar cells. Although this
423 border is well described for mammalian species, it remains unclear in birds since even the number of
424 strata is not entirely resolved (Millar et al., 1987; Naito and Chen, 2004; Ritchey et al., 2010). We used
425 antibodies against PKC alpha to label a subpopulation of putative ON bipolar cells (Ritchey et al., 2010)
426 (Fig. 6 grey), GNB3 as a putative marker for all ON bipolar cells (Ritchey et al., 2010) (Fig. 6 green) and
427 Ctbp2 to visualize all ribbon synapses in our tissue (Fig. 6 magenta). PKC positive cells were found to
428 be positive for GNB3, indicating that these cells are indeed ON bipolar cells (Fig. 6A-F). Comparing the
429 morphology and stratification levels of PKC positive bipolar cells with our 3D reconstructed cells, we
430 find a high similarity with B9 and B10 bipolar cells, which are exclusively contacting single cones. The
431 only difference between the PKC positive cells and the B9 or B10 bipolar cell types, respectively, is the
432 stratification in the inner most stratum (S6/7) which is more excessive in the PKC cells than in our

433 reconstructions. Additionally, if the GNB3 marker indeed labels the ON strata of the avian IPL and we
434 assume eight strata, then the border between OFF and ON would be between S3 and S4 (Fig. 6E, F).
435 Comparing the GNB3 staining with Ctbp2 labelling, we found that synapses in the supposed OFF
436 stratum 1 are GNB3 positive which indicates that ON bipolar cells also stratify in the distal OFF layer.
437 Likewise, we found Ctbp2 positive but GNB3 negative areas between S4 and S5, S6 and S7 and in S7
438 and S8 indicating that OFF bipolar cells stratify in the ON strata of the IPL as well (Fig. 6 I, J). This
439 eliminates the clear separation between ON and OFF signals in the IPL. If we apply this stratification
440 pattern to our reconstructed bipolar cells and combine it with the type of contacts a bipolar cell makes
441 to the photoreceptor terminals, we suggest that bipolar cells belonging to our groups B1, B3, B7, and
442 B8 are putative OFF bipolar cells, whereas the groups of B2, to B6, B9 and B10 are putative ON bipolar
443 cell candidates. Clearly, electrophysiological studies are needed to corroborate these putative
444 assignments.

445 **Discussion**

446 We obtained the first 3D electron microscopic dataset for the avian retina using ssmSEM. We used this
447 dataset to 1) revisit the anatomy of double cones, 2) present insights into double cone connectivity to
448 other photoreceptors, and 3) provide the first classification of avian bipolar cell types that considers
449 photoreceptor to bipolar cell connectivity. Additionally, we found a surprisingly large and diverse
450 number of photoreceptor-photoreceptor connections, which, to our knowledge, were not previously
451 described in such diversity in any bird, and a surprising number of inputs from several different
452 photoreceptor cells to most of the individual bipolar cell types.

453 **Photoreceptor-photoreceptor connections**

454 Evidence from mammals and fish suggests that telodendria contact each other and form gap junctions
455 (DeVries et al., 2002; Noel and Allison, 2018), which are thought to have various functions. Cone-cone
456 coupling e.g. correlates common light-mediated input and reduces noise from individual
457 photoreceptors by averaging across the coupled network (DeVries et al., 2002; O'Brien et al., 2012),

458 thereby increasing the signal-to-noise ratio. Rod-rod coupling was shown to enhance contrast
459 detection in dim light, at the cost of reducing absolute sensitivity (Li et al., 2012). Here, we found that
460 predominantly rod photoreceptors form tip-to-tip and tip-to-shaft telodendrial contacts (Fig. 3-1).
461 Since we were not able to identify gap junctions in our ssmSEM data set, we can only speculate that
462 rod-rod electrical coupling is more abundant than cone-cone or rod-cone coupling in the chicken and
463 that they may serve similar functions as in other vertebrate classes.

464 In turtles, rods and cones also form chemical synapses between telodendria and photoreceptor
465 terminals (Mariani and Lasansky, 1984; Kolb and Jones, 1985; Owen, 1985). Functional experiments in
466 tiger salamander also suggest that rods and cones are electrically and chemically coupled (Attwell et
467 al., 1983). Here, we report, for the first time in birds, that also chicken photoreceptor cells make
468 telodendrial contacts with other photoreceptor terminals. These contacts mainly involved one or both
469 members of a double cone and other photoreceptor cell types but also occurred between green/red
470 single cones.

471 Our data suggest that rod-rod coupling in the chicken retina could primarily be mediated by electrical
472 synapses whereas cone-cone or rod-cone connections could be mediated by chemical synapses. In
473 turtles, sites of chemical synapses between red and green cones were hypothesised to lead to an
474 excitatory colour mixing which was found in electrophysiological recordings (Kolb and Jones 1985).
475 Since rods and double cones are likely to be involved in luminance detection rather than colour vision
476 (Lind et al., 2014), the chemical synapses between these two photoreceptor types could serve to
477 enlarge the operational range of the luminance channel and thereby enhance its sensitivity.

478 **Bipolar cell classification and connectivity to photoreceptor cells**

479 The bipolar cell classification provided here comprises 15 different types. Interestingly, we found that
480 the axonal stratification pattern and photoreceptor connectivity were the most defining factors for the
481 types: bipolar cells with the same axonal arbour contacted different photoreceptors. This is similar to
482 the zebrafish retina (Li et al., 2012) but in contrast to the mammalian retina where the same axonal

483 stratification is associated with the same photoreceptor connectivity (Euler et al., 2014). The presence
484 or absence of a Landolt's club does not seem to be a defining feature because cells belonging to the
485 same bipolar cell type, based on uniform dendritic and axonal mosaics, can possess, or lack this special
486 protrusion (e.g., types 3a, 4c; Fig. 4-4 and 4-8). If the Landolt's club was a defining feature, we would
487 expect the mosaics to show higher inhomogeneity and overlap within our defined bipolar cell types.

488 For the retina of a tetrachromatic animal (Hart, 2001), it seems very surprising that most bipolar cells
489 make contacts to different photoreceptor cell types, thereby mixing colour channels. Furthermore,
490 most bipolar cell types seem to get most of their input from the principal member of double cones
491 (Fig. 4A; Fig. 4-1 to Fig.4-15). This may indicate that double cones are involved not only in luminance
492 detection, but also in colour vision, presumably processed in parallel bipolar cell pathways. Bipolar
493 cells in other animals contacting exclusively one type of single cone usually have wide dendritic fields
494 [e.g. in rabbit (MacNeil and Gaul, 2008) and mouse (Haverkamp et al., 2005)], and these are the ones
495 in our dataset which have reached the end of the volume more frequently than small-field bipolar cells.
496 Therefore, bipolar cells exclusively contacting individual photoreceptor types, i.e., presumed colour-
497 sensitive bipolar cells, may be underrepresented in our analysis which could explain the low number
498 of bipolar cell types contacting the B/V single cones. Nevertheless, it is surprising that only one bipolar
499 cell type contacted the B/V single cones whereas at least in zebrafish the UV single cones were found
500 to be frequently contacted by a large number of bipolar cells (Li et al., 2012). Bipolar cell type B5a may
501 represent a bird midget bipolar cell type. Primate midget bipolar cells are characterized by a very small
502 dendritic and axonal field and they contact only one single cone in the central retina (Polyak, 1941;
503 Puller et al., 2007). Therefore, midget bipolar cells mediate high-acuity vision (Euler et al., 2014). Since
504 our dataset is from peripheral chicken retina it might be possible that this cell type receives single cone
505 input in the area centralis. For other vertebrate retinas, it was proposed that bipolar cell types follow
506 a so called "block wiring", meaning that they contact spectrally neighbouring photoreceptor cells (red
507 and green) rather than leaving a spectral gap (red and blue) [for overview see (Baden and Osorio,

508 2019)]. Our data set also supports this hypothesis for the chicken retina, although we cannot separate
509 all single cone types.

510 Recently, a detailed analysis on chicken retinal cell types was performed using single cell
511 transcriptomics, and 22 different bipolar cells were identified (Yamagata et al., 2021), indicating that
512 we are missing 7 bipolar cell types. One reason could be the limited z-depth of our dataset which
513 potentially leads to a reduced number of wide-field bipolar cells. In addition, separating the R/G and
514 B/V group of single cones could also lead to a regrouping of the bipolar cell types. Compared to
515 previous anatomical studies, we were able to link all of the bipolar cell types identified in pigeon
516 (Mariani, 1987) to our data. We also found similarities to the identified bipolar cells in chicken retina,
517 but also identified new types (Quesada et al., 1988) (for detailed comparison see Fig.4-17).

518 In general, it is striking that all bipolar cell types are at least bistratified in the IPL whereas mammalian
519 bipolar cells are mostly monostратified (Euler et al., 2014) and also fish have a few monostратified cells
520 in addition to several multistratified types (Li et al., 2012). Since the border between the ON and OFF
521 layer in the IPL is not resolved in the chicken, we used the GNB3 staining as a reference for ON bipolar
522 cells (Ritchey et al., 2010) and Ctbp2 as ribbon synaptic marker. Combining the axonal stratification of
523 the identified bipolar cells with the immunostaining and the type of contacts the cells made to the
524 photoreceptor terminals, it is likely that OFF bipolar cells also stratify in the ON strata of the IPL as it
525 was demonstrated in turtle (Ammermüller and Kolb, 1995) and zebrafish retina (Connaughton, 2001).
526 Our Ctbp2 staining supports that hypothesis because we found ribbon synapses in GNB3-negative
527 strata in the ON part of the IPL. Additionally, OFF bipolar cells can form ribbon synapses with
528 photoreceptors (e.g. in fish (Saito et al., 1985; Sakai and Naka, 1983) and we cannot conclude that all
529 bipolar cells that make basal contacts are OFF cells because, in primates, ON bipolar cells also form
530 basal contacts with the photoreceptor terminal (Hopkins and Boycott, 1996). Thus, functional data are
531 needed to unequivocally decide which bipolar cell types are ON and OFF cells.

532 **Could the region in the retina change proportion of bipolar cell types or shape?**

533 Our dataset was recorded in the dorsal area of the left eye of a one-week old chicken (*Gallus gallus*
534 *domesticus*). The photoreceptor density and composition in the retina of birds and other animals
535 change from the periphery to the centre and can, in some cases, be divided into special areas (for
536 overview see (Seifert et al., 2020). Not only the ratio between the photoreceptor types change
537 between periphery and centre, the total number of photoreceptor cells and ganglion cells also
538 decrease from the centre to the periphery (Bueno et al., 2011). The increasing number of
539 photoreceptor cells could lead to a higher density of bipolar cells with smaller dendritic fields in the
540 central retina. Also, we cannot exclude that the central retina harbours bipolar cell types which have
541 been missing from the more peripheral area analyzed here. Additionally, it was reported that the left
542 eye is more involved in high spatial acuity tasks than the right eye (for review see Seifert et al. 2020),
543 indicating that the retinal wiring may differ between both eyes.

544 **Double cone anatomy**

545 The detailed reconstruction of an individual double cone largely confirmed previous data: 1) accessory
546 members show fragmented oil droplets, and 2) principal and accessory members are connected by
547 junction-like structures. These structures may, at first glance, contradict the idea that light-dependent
548 magnetoreception could be based on the differential signalling of avian double cones by expressing
549 two sensors arranged in different orientations (Hore and Mouritsen, 2016; Worster et al., 2017).
550 Electrically mixing the resulting signals already at the photoreceptor level seems counterintuitive.
551 However, as we do not know under which light conditions (Yang and Wu, 1989) or time of the day
552 (Ribelayga et al., 2008) the gap junction-like structures can pass signals, these gap junctions might be
553 closed under the light conditions when magnetoreception is most relevant. Further research should
554 investigate this issue.

555 **Conclusion**

556 Here, we present the first 3D reconstructed bird retina data set. We identified many previously
557 undescribed photoreceptor-photoreceptor connections in the chicken retina which suggests

558 numerous interactions between rods and cones as well as between different cones types at the first
559 stages of visual processing. We increased the number of morphologically known bipolar cell types from
560 11 to 17 and identified their complete connectivity to photoreceptor cells. Surprisingly, most bipolar
561 cell types contact several different photoreceptor cell types. Astoundingly, 13 out of 15 identified
562 bipolar cell types got at least part of their input from double cones. Therefore, our data suggest that
563 the double cones play many different and important roles in avian retinal processing and that the
564 neural network and thus information processing in the outer retina is in general much more complex
565 than previously expected.

566

567 **Author contributions**

568 Experiment Design and Supervision, H.M., K.D., S.I., A.G., S.H., K.B.; Experiments, A.G., S.I., S.H.; Data
569 Analysis, A.G., K.D., S.H., and H.M.; Writing, A.G., K.D., H.M., S.H., K.B.

570 **References**

571 Ammermüller J and Kolb H (1995) The Organization of the Turtle Inner Retina. I. ON- and OFF-Center
572 Pathways. *The Journal of Comparative Neurology* 358: 1–34.

573 Ammermüller J and Kolb H (1996) Functional Architecture of the Turtle Retina. *Progress in Retinal
574 and Eye Research* 15(2): 393–433.

575 Attwell D, Werblin FS, Wilson M and Wu SM (1983) A sign-reversing pathway from rods to double
576 cone and single cones in the retina of the tiger salamander. *The Journal of Physiology* 336: 313–
577 333.

578 Baden T and Osorio D (2019) The Retinal Basis of Vertebrate Color Vision. *Annual Reviews of Vision
579 Science* 5(3): 1–24.

580 Bowmaker JK (2008) Evolution of vertebrate visual pigments. *Vision Research* 48: 2022–2041. DOI:

- 581 10.1016/j.visres.2008.03.025.
- 582 Boycott BB and Wässle H (1991) Morphological Classification of Bipolar Cells of the Primate Retina.
583 *European Journal of Neuroscience* 3: 1069–1088.
- 584 Bueno JM, Giakoumaki A, Gualda EJ, Schaeffel F and Artal P (2011) Analysis of the chicken retina with
585 an adaptive optics multiphoton microscope. *Biomedical optics express* 2(6): 1637–1648.
- 586 Calkins DJ, Tsukamoto Y and Sterling P (1996) Foveal Cones form Basal as well as Invaginating
587 Junctions with Diffuse ON Bipolar Cells. *Vision Research* 36(21): 3373–3381.
- 588 Chernetsov N, Pakhomov A, Kobylkov D, Kishkinev D, Holland RA and Mouritsen H (2017) Migratory
589 Eurasian Reed Warblers Can Use Magnetic Declination to Solve the Longitude Problem. *Current*
590 *Biology* 27. Elsevier Ltd.: 1–5. DOI: 10.1016/j.cub.2017.07.024.
- 591 Cohen AI (1960) The Ultrastructure of the Rods of the Mouse Retina. *American Journal for Anatomy*
592 107: 23–48.
- 593 Cohen AI (1972) Rods and Cones. In: Fuortes M (ed.) *Handbook of Sensory Physiology* VII/2.
594 *Physiology of Photoreceptors Organs*. Berlin: Springer-Verlag, pp. 63–110.
- 595 Connaughton VP (2001) Organization of ON- and OFF-pathways in the zebrafish retina :
596 neurotransmitter localization , electrophysiological responses of bipolar cells , and patterns of
597 axon terminal stratification. In: Kolb H and Ripps H (eds) *Progress in Brain Research*, pp. 161–
598 176.
- 599 DeVries SH, Qi X, Smith RG, Makous W and Sterling P (2002) Electrical Coupling between Mammalian
600 Cones. *Current biology* 12(02): 1900–1907.
- 601 Dowling JE and Boycott BB (1966) Organization of the primate retina : electron microscopy.
602 *Proceedings of the Royal Society London B* 166(1002): 80–111.
- 603 Drenhaus U, Morino P and Veh RW (2003) On the Development of the Stratification of the Inner
604 Plexiform Layer in the Chick Retina. *The Journal of Comparative Neurology* 460: 1–12. DOI:

- 605 10.1002/cne.10602.
- 606 Drenhaus U, Voigt T and Rager G (2007) Onset of Synaptogenesis in the Plexiform Layers of the Chick
607 Retina : A Transmission Electron Microscopic Study. *Microscopy reasearch and technique* 70:
608 329–335. DOI: 10.1002/jemt.
- 609 Eberle AL, Mikula S, Schalek R, Lichtman JW, Knothe Tate ML and Zeidler D (2015) High-resolution ,
610 high-throughput imaging with a multibeam scanning electron microscope. *Journal of*
611 *Microscopy* 259(2): 114–120. DOI: 10.1111/jmi.12224.
- 612 Eberle AL and Zeidler D (2018) Multi-Beam Scanning Electron Microscopy for High-Throughput
613 Imaging in Connectomics Research. *frontiers in Neuroanatomy* 12(112): 1–7. DOI:
614 10.3389/fnana.2018.00112.
- 615 Ebrey T and Koutalos Y (2001) Vertebrate Photoreceptors. *Progress in Retinal and Eye Research*
616 20(1): 49–94.
- 617 Euler T, Haverkamp S, Schubert T, et al. (2014) Retinal bipolar cells : elementary building blocks of
618 vision. *Nature Reviews Neuroscience* 15. Nature Publishing Group: 507–519. DOI:
619 10.1038/nrn3783.
- 620 Ghosh KK, Martin PR and Grünert U (1997) Morphological Analysis of the Blue Cone Pathway in the
621 Retina of a New World Monkey , the Marmoset *Callithrix jacchus*. *The Journal of Comparative*
622 *Neurology* 379: 211–225.
- 623 Günther A, Einwich A, Sjulstok E,Feederle R, Bolte P, Koch K-W, Solov'yov IA and Mouritsen H (2018)
624 Double-Cone Localization and Seasonal Expression Pattern Suggest a Role in Magnetoreception
625 for European Robin Cryptochrome 4. *Current Biology* 28: 1–13. DOI: 10.1016/j.cub.2017.12.003.
- 626 Hart NS (2001) The Visual Ecology of Avian Photoreceptors. *Progress in Retinal and Eye Research*
627 20(5): 675–703.
- 628 Haverkamp S, Grünert U and Wässle H (2000) The Cone Pedicle , a Complex Synapse in the Retina.

- 629 *Neuron* 27: 85–95.
- 630 Haverkamp S, Wässle H, Duebel J, Kuner T, Augustine GJ, Feng G and Euler T (2005) The Primordial ,
631 Blue-Cone Color System of the Mouse Retina. *The Journal of Neuroscience* 25(22): 5438–5445.
632 DOI: 10.1523/JNEUROSCI.1117-05.2005.
- 633 Hering H and Kröger S (1996) Formation of Synaptic Specializations in the Inner Plexiform Layer of
634 the Developing Chick Retina. *The Journal of Comparative Neurology* 375: 393–405.
- 635 Higham DJ and Higham NJ (2016) *MATLAB Guide*. Philadelphia. Society for Industrial and Applied
636 Mathematics.
- 637 Hopkins JM and Boycott BB (1996) The cone synapses of DB1 diffuse, DB6 diffuse and invaginating
638 midget, bipolar cells of a primate retina. *Journal of Neurocytology* 25(7): 381–390.
- 639 Hore PJ and Mouritsen H (2016) The Radical-Pair Mechanism of Magnetoreception. *Annual Review of*
640 *Biophysics* 45: 299–344. DOI: 10.1146/annurev-biophys-032116-094545.
- 641 Hornstein EP, Verweij J, Li PH and Schnapf JL (2005) Gap-Junctional Coupling and Absolute Sensitivity
642 of Photoreceptors in Macaque Retina. *The Journal of Neuroscience* 25(48): 11201–11209. DOI:
643 10.1523/JNEUROSCI.3416-05.2005.
- 644 Horváth G (2014) *Polarized Light and Polarization Vision in Animal Sciences*. second edi. Berlin:
645 Springer Verlag. DOI: 10.1007/978-3-642-54718-8.
- 646 Hua Y, Laserstein P and Helmstaedter M (2015) Large-volume en-bloc staining for electron
647 microscopy-based connectomics. *Nature Communications* 6,7923. DOI: 10.1038/ncomms8923.
- 648 Jones CD and Osorio D (2004) Discrimination of oriented visual textures by poultry chicks. *Vision* 44:
649 83–89. DOI: 10.1016/j.visres.2003.08.014.
- 650 Kihara AH, Paschon V, Cardoso CM, Higa GSV, Castro LM, Hamassaki DE and Britto LRG (2009)
651 Connexin36 , an Essential Element in the Rod Pathway , Is Highly Expressed in the Essentially
652 Rodless Retina of Gallus gallus. *The Journal of Comparative Neurology* 512: 651–663. DOI:

- 653 10.1002/cne.21920.
- 654 Kishkinev D, Chernetsov N, Pakhomov A, Heyers D and Mouristen H (2015) Eurasian reed warblers
655 compensate for virtual magnetic displacement. *Current Biology* 25: R822–R824. DOI:
656 10.1016/j.cub.2015.08.012.
- 657 Kolb H (1977) The organization of the outer plexiform layer in the retina of the cat : electron
658 microscopic observations. *Journal of Neurocytology* 6: 131–153.
- 659 Kolb H and Jones J (1985) Electron Microscopy of Golgi-Impregnated Photoreceptors Reveals
660 Connections Between Red and Green Cones in the Turtle Retina. *Journal of Neurophysiology*
661 54(2): 304–317.
- 662 Kremer JR, Mastronarde DN and McIntosh JR (1996) Computer Visualization of Three-Dimensional
663 Image Data Using IMOD. *Journal of Structural Biology* 116(0013): 71–76.
- 664 Ladman AJ (1958) The Fine Structure of the Rod-Bipolar Cell Synapse in the Retina of the Albino Rat.
665 *Journal of Biophysics and Biochemistry* 4(4): 459–466.
- 666 Lagnado L and Schmitz F (2015) Ribbon Synapses and Visual Processing in the Retina. *Annual Review*
667 *of Vision Science* 1: 235–262. DOI: 10.1146/annurev-vision-082114-035709.
- 668 Li H, Chuang AZ and Brien JO (2009) Photoreceptor Coupling Is Controlled by Connexin 35
669 Phosphorylation in Zebrafish Retina. *The Journal of Neuroscience* 29(48): 15178–15186. DOI:
670 10.1523/JNEUROSCI.3517-09.2009.
- 671 Li W and DeVries SH (2006) Bipolar cell pathways for color and luminance vision in a dichromatic
672 mammalian retina. *Nature Neuroscience* 9(5): 669–675. DOI: 10.1038/nn1686.
- 673 Li YN, Tsujimura T, Kawamura S and Dowling JE (2012) Bipolar Cell-Photoreceptor connectivity in the
674 zebrafish (*Danio rerio*) retina. *Journal of Comparative Neurology* 520(16): 3786–3802. DOI:
675 10.1002/cne.23168.Bipolar.
- 676 Lind O and Kelber A (2011) The spatial tuning of achromatic and chromatic vision in budgerigars.

- 677 *Journal of Vision* 11(7): 1–9. DOI: 10.1167/11.7.2.
- 678 Lind O, Chavez J and Kelber A (2014) The contribution of single and double cones to spectral
679 sensitivity in budgerigars during changing light conditions. *Journal of Comparative Physiology A*
680 200: 197–207. DOI: 10.1007/s00359-013-0878-7.
- 681 López-López R, López-Gallardo M, Pérez-Álvarez MJ, et al. (2008) Isolation of chick retina cones and
682 study of their diversity based on oil droplet colour and nucleus position. *Cell Tissue Research*
683 332: 13–24. DOI: 10.1007/s00441-007-0572-6.
- 684 MacNeil MA and Gaul PA (2008) The biocytin wide-field bipolar cell in the rabbit retina selectively
685 contacts blue cones. *Journal for Comparative Neurology* 506(1): 6–15. DOI: 10.1002/cne.21491.
- 686 Mariani AP (1984) Bipolar cells in monkey retina selective for the cones likely to be blue-sensitive.
687 *Nature* 308: 184–186.
- 688 Mariani AP (1987) Neuronal and Synaptic Organization of the Outer Plexiform Layer of the Pigeon
689 Retina. *The american journal of anatomy* 179: 25–39.
- 690 Mariani AP and Lasansky A (1984) Chemical synapses between turtle photoreceptors. *Brain Research*
691 310: 351–354.
- 692 Mariani AP and Leure-du Pree AE (1978) Photoreceptors and Oil Droplet Colors in the Red Area of the
693 Pigeon Retina. *Journal for Comparative Neurology* 182: 821–838.
- 694 Meller K (1964) Elektronenmikroskopische Befunde zur Differenzierung der Photorezeptorzellen und
695 Bipolarzellen der Retina und ihrer synaptischen Verbindungen. *Zeitschrift für Zellforschung* 64:
696 733–750.
- 697 Mey J and Thanos S (2000) Development of the visual system of the chick I. Cell differentiation and
698 histogenesis. *Brain Research Reviews* 32: 343–379.
- 699 Meyer DB and May HJ (1973) The Topographical Distribution of Rods and Cones in the Adult
700 Chicken Retina. *Experimental Eye Research* 17: 347–355.

- 701 Millar TJ, Ishimoto I, Chubb IW, et al. (1987) Cholinergic amacrine cells of the chicken retina: A light
702 and electron microscope immunohistochemical study. *Neuroscience* 21(3): 725–743.
- 703 Mouritsen H (2018) Long-distance navigation and magnetoreception in migratory animals. *Nature*
704 558. Springer US: 50–59. DOI: 10.1038/s41586-018-0176-1.
- 705 Naito J and Chen Y (2004) Morphologic Analysis and Classification of Ganglion Cells of the Chick
706 Retina by Intracellular Injection of Lucifer Yellow and Retrograde Labeling with Dil. *The Journal*
707 *of Comparative Neurology* 469: 360–376. DOI: 10.1002/cne.11010.
- 708 Nishimura Y, Smith RL and Shimai K (1981) Junction-like structure appearing at apposing membranes
709 in the double cone of chick retina. *Cell Tissue Research* 218: 113–116.
- 710 Noel NCL and Allison WT (2018) Connectivity of cone photoreceptor telodendria in the zebrafish
711 retina. *Journal of Comparative Neurology* 526: 609–625. DOI: 10.1002/cne.24354.
- 712 O’Brien JJ, Chen X, MacLeish PR, et al. (2012) Photoreceptor Coupling Mediated by Connexin36 in the
713 Primate Retina. *The Journal of Neuroscience* 32(13): 4675–4687. DOI:
714 10.1523/JNEUROSCI.4749-11.2012.
- 715 Osorio D and Vorobyev M (2005) Photoreceptor spectral sensitivities in terrestrial animals :
716 adaptations for luminance and colour vision. *Proceedings of the Royal Society London B* 272:
717 1745–1752. DOI: 10.1098/rspb.2005.3156.
- 718 Owen WG (1985) Chemical and Electrical Synapses Between Photoreceptors in the Retina of the
719 Turtle , *Chelydra serpentina*. *The Journal of Comparative Neurology* 240: 423–433.
- 720 Peddie CJ and Collinson LM (2014) Exploring the third dimension : Volume electron microscopy
721 comes of age. *Micron* 61. Elsevier Ltd: 9–19. DOI: 10.1016/j.micron.2014.01.009.
- 722 Pedler CMH and Boyle M (1969) Multiple oil droplets in the photoreceptors of the pigeon. *Vision*
723 *Research* 9: 525–528.
- 724 Polyak SL (1941) *The Retina: The Anatomy and the Histology of the Retina in Man, Ape, and Monkey*,

- 725 *Including the Consideration of Visual Functions, the History of Physiological Optics, and the*
726 *Histological Laboratory Technique*. Chicago: University of Chicago Press.
- 727 Puller C, Haverkamp S and Gru U (2007) OFF Midget Bipolar Cells in the Retina of the Marmoset ,
728 *Callithrix jacchus* , Express AMPA Receptors. *The Journal of Comparative Neurology* 502: 442–
729 454. DOI: 10.1002/cne.
- 730 Quesada A, Prada FA and Genis-Galvez JM (1988) Bipolar Cells in the Chicken Retina. *Journal of*
731 *morphology* 197: 337–351.
- 732 Ribelayga C, Cao Y and Mangel SC (2008) The circadian clock in teh retina controls rod-cone coupling.
733 *Neuron* 59(5): 790–801. DOI: 10.1016/j.neuron.2008.07.017.The.
- 734 Ritchey ER, Bongini RE, Code KA, Zelinka C, Peterson-Jones S and Fischer AJ (2010) The pattern of
735 expression of gunaine nucleotide-binding protein beta3 (GNB3) in the retina is conserved across
736 vertebrate species. *Neuroscience* 169(3): 1376–1391. DOI:10.1016/j.neuroscience.2010.05.081.
- 737 Saito T, Kujiraoka T, Yonaha T and Chino J (1985) Reexamination of Photoreceptor-Bipolar
738 Connectivity Patterns in Carp Retina : HRP-EM and Golgi-EM Studies. *The Journal of*
739 *Comparative Neurology* 236: 141–160.
- 740 Sakai H and Naka K-I (1983) Synaptic organisation involving receptor, horizontal and ON- and OFF-
741 center bipolar cells in the catfish retina. *Vision Research* 23(4): 339–351.
- 742 Schindelin J, Arganda-Carreras I, Frise E, Kaynig V, Longair M, Pietzsch T, Preibisch S, Rueden C,
743 Saalfeld S, Schmid B, Tinevez J-Y, White DJ, Hartenstein V, Eliceiri K, Tomancak P and Cardona A
744 (2012) Fiji : an open-source platform for biological-image analysis. *Nature Methods* 9(7): 676–
745 682. DOI: 10.1038/nmeth.2019.
- 746 Seifert M, Baden T and Osorio D (2020) The retinal basis of vision in chicken. *Seminars in Cell and*
747 *Developmental Biology*. Elsevier. DOI: 10.1016/j.semcdb.2020.03.011.
- 748 Stavenga DG and Wilts BD (2014) Oil droplets of bird eyes : microlenses acting as spectral filters.

- 749 *Philosophical Transactions of the Royal Society B* 369(20130041). DOI:
750 <http://dx.doi.org/10.1098/rstb.2013.0041>.
- 751 Tanabe K, Takahashi Y, Sato Y, et al. (2006) Cadherin is required for dendritic morphogenesis and
752 synaptic terminal organization of retinal horizontal cells. *Development* 133: 4085–4096. DOI:
753 10.1242/dev.02566.
- 754 Tsukamoto Y and Omi N (2015) OFF bipolar cells in macaque retina : type-specific connectivity in the
755 outer and inner synaptic layers. *frontiers in Neuroanatomy* 9(122). DOI:
756 10.3389/fnana.2015.00122.
- 757 Tsukamoto Y and Omi N (2017) Classification of Mouse Retinal Bipolar Cells : Type-Specific
758 Connectivity with Special Reference to Rod-Driven All Amacrine Pathways. *frontiers in*
759 *Neuroanatomy* 11(92): 1–25. DOI: 10.3389/fnana.2017.00092.
- 760 Waldvogel JA (1990) The Bird's Eye View. *American Scientist* 78(4): 342–353.
- 761 Walls GL (1942) *The Vertebrate Eye and Its Adaptive Radiation*. New York: Hafner.
- 762 Wässle H, Puller C, Müller F and Haverkamp S (2009) Cone Contacts , Mosaics , and Territories of
763 Bipolar Cells in the mouse retina. *The Journal of Neuroscience* 29(1): 106–117. DOI:
764 10.1523/JNEUROSCI.4442-08.2009.
- 765 Wiltschko R and Wiltschko W (1995) *Magnetic Orientation in Animals*. Berlin Heidelberg: Springer
766 Verlag.
- 767 Wood AC (1917) The fundus oculi of birds especially as viewed by the ophthalmoscope. *The*
768 *Lakeside Press*.
- 769 Worster S, Mouritsen H and Hore PJ (2017) A light-dependent magnetoreception mechanism
770 insensitive to light intensity and polarization. *Journal of the Royal Society, Interface* 14:
771 20170405. DOI: <http://dx.doi.org/10.1098/rsif.2017.0405>.
- 772 Yamagata M, Yan W and Sanes JR (2021) A cell atlas of the chick retina based on single-cell

- 773 transcriptomics. *eLife* 10:e63907.
- 774 Yang X-L and Wu SM (1989) Modulation of Rod-Cone Coupling by Light. *Science* 244(4902): 352–354.
- 775 Zapka M, Heyers D, Hein CM, Engels S, Schneider N-L, Hans J, Weiler S, Dreyer D, Kishkinev D, Wild
776 JM and Mouritsen H (2009) Visual but not trigeminal mediation of magnetic compass
777 information in a migratory bird. *Nature* 461: 1274–1278. DOI: 10.1038/nature08528.
- 778 Zoltowski BD, Chelliah Y, Wickramaratne A, et al. (2019) Chemical and structural analysis of a
779 photoactive vertebrate cryptochrome from pigeon. *Proceedings of the National Academy of*
780 *Sciences* 116(39): 19449–19457. DOI: 10.1073/pnas.1907875116.
- 781
- 782

783 **Figure 1. 3D reconstructed sub-volume used for bipolar and photoreceptor cell connectivity**
784 **analysis. (A)** 3D volume representation of the original EM data set highlighting the dimensions of the
785 data set. **(B)** Model representation of all double cones (principal member in dark blue and accessory
786 member in bright blue), rods (brown), green/red cones (green) and blue/violet single cones
787 (magenta) as well as all complete bipolar cell grouped in the identified bipolar cell types indicated in
788 different shades of yellow-orange-red-violet. **(C)** Bottom view of double cone (principal member in
789 dark blue and accessory member in bright blue) terminals. **(D)** Bottom view of green/red cone
790 (green) and blue/violet cone (magenta) terminals **(E)** Bottom view of rod terminals (brown). **(F)** Front
791 view of all photoreceptor cell types within the volume with OPL lamina highlighted. Examples for the
792 trackability of the data set are given in Figure 1-1 including an outline of a complete section with the
793 highlighted sub-volumes. PR = principal member, AC = accessory member, G/R = green/red single
794 cones, B/V = blue/violet single cones.

795 **Figure 1-1. Trackability of cells through the gap between slice 72 and 73. (A)** Schematic representation
796 of a x/y slice from the sub-volume used for bipolar cell reconstruction highlighting positions for
797 examples to check for trackability through the gap. **(B and C)** EM images from the OPL showing the
798 slice before and after the lost slices for comparison. Large features can be used as landmarks in order
799 to track smaller structures as well. **(D and E)** EM images representing example positions in the IPL to
800 compare the slice before and after the gap. Most of the structures can be tracked through the gap;
801 only thin, sideways moving structures were sometimes lost. **(F)** Example section of the dataset.
802 Complete section used for photoreceptor cell types abundance. Highlighted are the subvolumes for
803 single double cone reconstruction (1) and bipolar cell and photoreceptor connectivity (2). ONL= outer
804 nuclear layer, OPL= outer plexiform layer, INL= inner nuclear layer, IPL= inner plexiform layer, GCL=
805 ganglion cell layer. Scale bar B-E: 2 μm , F: 100 μm .

806

807 **Figure 2. Double cone anatomy in the chicken retina. (A)** 3D reconstruction of both members of a
808 double cone, principal member (blue) and accessory member (pale orange) from the outer segments

809 containing densely packed disc membranes to the photoreceptor terminal where the signal transfer
810 occurs. The oil droplets in both members (green) are located in the inner segments directly at the
811 border to the outer segments. In the accessory member multiple small oil droplets or granules could
812 be found. The more than 200 mitochondria per cell (yellow) are densely packed in the ellipsoid part
813 of the inner segment. The golgi apparatus (red) is located in the myoid part of the inner segment
814 close to the nucleus (magenta). The accessory member of the double cone additionally contains a
815 paraboloid (dark orange) in the myoid part of the inner segment. **(B)** TEM image of the outer
816 segment of an accessory member from a double cone. Densely packed discs are visible as well as two
817 of multiple oil droplets and calycal processes on both sides of the outer segment indicated by the
818 arrows. **(C)** Magnified area from (B) reveals the typical invaginations formed in the outer segments of
819 cones (arrow). **(D)** TEM images of the outer membranes of both double cone members which form
820 junction-like structures (arrow) along the inner segments. **(E)** TEM image of a ribbon synapse in the
821 principal member of a double cone terminal. AC = accessory member, PR = principal member, HC =
822 horizontal cell dendrite, BC = invaginating bipolar cell dendrite. Scale bars: B = 2 μm , C and D = 100
823 nm, E = 200 nm.

824

825 **Figure 3. Connections from the double cone to other photoreceptors.** The two images on the left
826 show front and bottom view of two neighboring 3D reconstructed photoreceptor terminals. **(A)**
827 Contacts between the PRs of neighboring double cones (dark and bright blue). The EM images on the
828 right show that both PRs make basal contacts in the neighboring PR terminal (white arrows). **(B)**
829 Contacts between the accessory member (AC, turquoise) and principal member (PR, dark blue) of a
830 double cone. The EM image on the right shows that double cone members make basal contacts in
831 the other member's terminal, and that the AC additionally makes contacts through ribbon synapses
832 in the PR terminal (white arrows). **(C)** Contact between the AC (turquoise) and a G/R cone (green).
833 The two images on the left indicate that only the AC makes a contact to the G/R cone terminal but

834 not the other way around. The EM image on the right shows that the AC makes a ribbon synapse
835 contact to the G/R cone terminal. **(D)** Contact between the PR of a double cone and a B/V cone. The
836 two images on the left indicate that only the B/V cone makes contacts to the PR terminal whereas
837 the PR does not seem to contact the B/V cone terminal. The EM image on the right shows that the
838 B/V cone makes multiple basal contacts to the PR terminal. **(E)** Contacts between PR and rods. The
839 EM images show that only the rod makes a basal contact with the PR terminal, but not the other way
840 around. **(F)** Connectivity matrix with percental representations (see method section) of presynaptic
841 basal contacts from PR (total # contacts=248), AC (total # contacts=26), rods (total # contacts=3), G/R
842 (total # contacts=180) and B/V (total # contacts=12). **(G)** Connectivity matrix with percental
843 representations of postsynaptic basal contacts from PR (total # contacts=100), AC (total #
844 contacts=96), rods (total # contacts=79), G/R (total # contacts=151) and B/V (total # contacts=43). **(H)**
845 Connectivity matrix with percental representations of presynaptic ribbon contacts from PR (total #
846 contacts=45), AC (total # contacts=0), rods (total # contacts=0), G/R (total # contacts=35) and B/V
847 (total # contacts=0). **(I)** Connectivity matrix with percental representations of postsynaptic ribbon
848 contacts from PR (total # contacts=0), AC (total # contacts=48), rods (total # contacts=0), G/R (total #
849 contacts=31) and B/V (total # contacts=1). Tip-to-tip and tip-to-shaft photoreceptor contacts are
850 shown in Figure 3-1 and the synaptic connectivity of a principal member terminal is shown in Figure
851 3-2. All photoreceptor cell contacts are shown in Figure 3-3 to Figure 3-6. G/R= green/red single
852 cones, B/V= blue/violet single cones. All scale bars = 2 μm .

853

854 **Figure 3-1. Telodendrial contacts between photoreceptor/photoreceptor within the chicken retina.**

855 (A) Example of a tip-to-tip contact between two photoreceptor telodendria. (B) Example of a tip-to-
856 shaft contact between two photoreceptor telodendria. (C) Connectivity matrix representing the
857 fractional number (see method section) of tip-to-tip contacts between telodendria from PR (total #
858 contacts=6), AC (total # contacts=0), rods (total # contacts=60), G/R (total # contacts=2) and B/V
859 (total # contacts=0). (D) Connectivity matrix representing the fractional number of tip-to-shaft

860 contacts between telodendria from PR (total # contacts=8), AC (total # contacts=0), rods (total #
861 contacts=24), G/R (total # contacts=20) and B/V (total # contacts=5). PR= Principal member of a
862 double cone, AC= accessory member of a double cone, G/R= green and red single cones, B/V= blue
863 and violet single cones.

864

865 **Figure 3-2. Synaptic connectivity of photoreceptors cell types. (A)** Schematic representation of a
866 principal member terminal showing the positions and types of each photoreceptor contact within the
867 terminal. Basal contacts represented by triangles; ribbon synapses represented by ovals. Length of
868 ovals represents size of ribbon synapse. **(B)** Schematic representation of principal member terminal
869 showing the positions and types of each bipolar cell contact within the terminal. **(C)** Front view of a
870 principal member terminal (blue) with exemplary basal and ribbon synaptic contacts (grey). All scale
871 bars = 2 μm . PR= principal member, AC= accessory member.

872

873 **Figure 3-3. Contacts of double cone members to other photoreceptor cells.** Principal and accessory
874 members from all double cones in the sub-volume are listed with all their different types of contacts
875 to other photoreceptor cells. Number of synapses are represented in the form (x/y) where x
876 represents the basal contacts and y the ribbon contacts. If displayed as (x) only basal contacts
877 occurred. The table also shows number of telodendria which reached the end of the volume or which
878 made no clear contacts meaning that the telodendria ended in the OPL without making any clear
879 contact to any cell.

880

881 **Figure 3-4. Contacts of rods to other photoreceptors.** All rods from the sub-volume are listed with all
882 their different types of contacts to other photoreceptor cells. Number of synapses are represented in
883 the form (x/y) where x represents the basal contacts and y the ribbon contacts. If displayed as (x)
884 only basal contacts occurred. The table also shows number of telodendria which reached the end of

885 the volume or which made no clear contacts meaning that the telodendria ended in the OPL without
886 making any clear contact to any cell. Rod 16 was excluded from the statistical evaluation because
887 only a very small part of the cell was in the volume.

888

889 **Figure 3-5. Contacts of G/R single cones to other photoreceptor cells.** All G/R cones in the sub-
890 volume are listed with all their different types of contacts to other photoreceptor cells. Number of
891 synapses are represented in the form (x/y) where x represents the basal contacts and y the ribbon
892 contacts. If displayed as (x) only basal contacts occurred. The table also shows number of telodendria
893 which reached the end of the volume or which made no clear contact meaning that the telodendria
894 ended in the OPL without making any clear contact to any cell.

895

896 **Figure 3-6. Contacts of B/V single cones to other photoreceptor cells.** All B/V single cones in the
897 sub-volume are listed with all their different types of contacts to other photoreceptor cells. Number
898 of synapses are represented in the form (x/y) where x represents the basal contacts and y the ribbon
899 contacts. If displayed as (x) only basal contacts occurred. The table also shows number of telodendria
900 which reached the end of the volume or which made no clear contact meaning that the telodendria
901 ended in the OPL without making any clear contact to any cell.

902

903 **Figure 4. Bipolar cell types in the chicken retina. (A)** Bipolar cell types are sorted based on their
904 axonal stratification level in the IPL. Below each bipolar cell type, the numbers of cells within this cell
905 type are shown, including their abundance within the bipolar cell class. Contacted photoreceptor
906 types are highlighted with respective color. Number of contacted photoreceptor cells and combined
907 mean number of basal and ribbon contacts per photoreceptor below. **(B-D)** Mean numbers of ribbon
908 and basal contacts per photoreceptor terminal for bipolar cell types B2, B5a and B7. Figures also
909 shown in Fig. 4-3, 4-9 and 4-12 for overall bipolar cell type summary. **(E-G)** Histograms showing the

910 averaged proportion of the three different classes of basal contacts (triad-associated, TA; marginal
911 and middle non-triad associated, NTA) of bipolar cell types B2, B5a and B7. Figures also shown in Fig.
912 4-3, 4-9 and 4-12 in the overall bipolar cell type summary. Analyses of each bipolar cell type are
913 represented in Figure 4-1 to 4-16 and a comparison between identified bipolar cells in this study and
914 other publications is shown in Figure 4-17. OPL = outer plexiform layer, INL = inner nuclear layer, IPL
915 = inner plexiform layer, PR = principal member, AC = accessory member, G/R= green/red single
916 cones; B/V = blue/violet single cones.

917

918 **Figure 4-1. Characterization of bipolar cell type B1a. (A)** 3D volume reconstruction of complete
919 bipolar cells from this type. Number of contacted photoreceptors and number of contacts per
920 photoreceptor terminal are indicated below each cell. Numbers of synapses are represented in the
921 form (x/y) where x represents the basal contacts and y the ribbon contacts. If displayed as (x), only
922 basal contacts occurred. **(B)** Mean cell density representation for B1a bipolar cells (yellow) based on
923 the volume of all cells from this bipolar cell type along the IPL depth. The sum of all mean bipolar cell
924 type densities in the IPL (black) indicates that strata 3, 5 and 8 are only weakly occupied by bipolar
925 cell axons. **(C)** Dendritic and axonal field mosaics of identified bipolar cell types. Front view of all
926 bipolar cells, which belong to one bipolar cell type, showing the overall distribution of the cells in the
927 data set. Dendrites are shown from a top view including dendritic fields, which are represented
928 through convex hull estimations to show dendritic field mosaic. Axonal fields are shown for each
929 stratum in the inner plexiform layer and are represented through convex hulls **(D)** Correlation
930 between missing branches and number of contacts/bipolar cell indicates that the number of contacts
931 does not decrease with an increase of missing branches. **(E)** Mean numbers of ribbon and basal
932 contacts per photoreceptor type terminal. One way ANOVA including Tukey test reveals that the
933 most contacted terminal from the principal member of a double cone has significantly more contacts
934 than the second most contacted terminal. Therefore, B1a bipolar cells contact predominantly one
935 principal member of a double cone and make less contacts to other principal members. **(F)** Histogram

936 showing the averaged proportion of the three different classes of basal contacts for each
937 photoreceptor cell type based on the classification by Tsukamoto and Omi (2015). **(G)** Distribution of
938 different types of synapses at the dendrite of one B1a bipolar cell (marked with two asterisks in A).
939 Basal contacts are represented as triangles and ribbon contacts as squares. Colors indicate type of
940 contacted photoreceptor cell; photoreceptor terminals are also represented in the corresponding
941 colors. B1a bipolar cells make most of their contacts to one central principal member of a double
942 cone and in significantly lower numbers also contacts to other photoreceptor cell types. OPL = outer
943 plexiform layer, INL = inner nuclear layer, IPL= inner plexiform layer, PR = Principal member of a
944 double cone, BC = bipolar cell, AC = accessory member of a double cone,
945 G/R = green and red single cones, B/V = blue and violet single cones, TA = triad associated, NTA =
946 non triad associated. Scale bar: G= 5 μ m.

947

948 **Figure 4-2. Characterization of bipolar cell type B1b.** **(A)** 3D volume reconstruction of complete
949 bipolar cells from this type. Same representation as in Fig.4-1. **(B)** Profile sum calculation for B1b
950 bipolar cells (orange) and profile sum of all bipolar cell types (black) in the IPL. **(C)** Dendritic and
951 axonal field mosaics of identified bipolar cell types. **(D)** Correlation between missing branches and
952 number of contacts/bipolar cell. **(E)** Mean numbers of ribbon and basal contacts per photoreceptor
953 terminal from each photoreceptor cell type. Due to a cell number of 2 it was not possible to perform
954 any statistical analysis. **(F)** Histogram showing the averaged proportion of the three different classes
955 of basal contacts. **(G)** Distribution of different types of synapses at the dendrite of one B1b bipolar
956 cell (** in A). Dendrites (orange) make basal (triangle) contacts. Colors indicate type of
957 photoreceptor cell that is contacted. OPL = outer plexiform layer, INL = inner nuclear layer, IPL= inner
958 plexiform layer, PR = Principal member of a double cone, BC = bipolar cell, AC = accessory member of
959 a double cone, G/R = green and red single cones, B/V = blue and violet single cones, TA = triad
960 associated, NTA = non triad associated. Scale bar: G= 5 μ m.

961

962 **Figure 4-3. Characterization of bipolar cell type B2. (A)** 3D volume reconstruction of complete
963 bipolar cells from this type. Partial bipolar cells that could be assigned to this bipolar cell type are
964 displayed as well. **(B)** Profile sum calculation for B2 bipolar cells (orange) and profile sum of all
965 bipolar cell types (black) in the IPL. **(C)** Dendritic and axonal field mosaics of identified bipolar cell
966 types. **(D)** Correlation between missing branches and number of contacts/bipolar cell indicates that
967 the number of contacts does not decrease with an increase of missing branches. **(E)** Mean numbers
968 of ribbon and basal contacts per photoreceptor terminal from each photoreceptor cell type.
969 Photoreceptor terminals are not significantly contacted with different numbers of contacts. **(F)**
970 Histogram showing the averaged proportion of the three different classes of basal contacts. **(G)**
971 Distribution of different types of synapses at the dendrite of one B2 bipolar cell (** in A). Dendrites
972 (orange) make both basal (triangles) and ribbon (squares) contacts. OPL = outer plexiform layer, INL =
973 inner nuclear layer, IPL= inner plexiform layer, PR = Principal member of a double cone, BC = bipolar
974 cell, AC = accessory member of a double cone, G/R = green and red single cones, B/V = blue and
975 violet single cones, TA = triad associated, NTA = non triad associated. Scale bar: G= 5 μ m.

976
977 **Figure 4-4. Characterization of bipolar cell type B3a. (A)** 3D volume reconstruction of complete
978 bipolar cells from this type. Partial bipolar cells that could be assigned to this bipolar cell type are
979 displayed as well. **(B)** Profile sum calculation for B3a bipolar cells (orange) and profile sum of all
980 bipolar cell types (black) in the IPL. **(C)** Dendritic and axonal field mosaics of identified bipolar cell
981 types. **(D)** Correlation between missing branches and number of contacts/bipolar cell indicates that
982 the number of contacts does not decrease with an increase of missing branches. **(E)** Mean numbers
983 of ribbon and basal contacts per photoreceptor terminal from each photoreceptor cell type. One way
984 ANOVA including Tukey test reveals that the most contacted terminal from the principal member of a
985 double cone has significantly more contacts than the second most contacted terminal. Therefore,
986 B3a bipolar cells contact predominantly one principal member of a double cone and make less
987 contacts to other principal members. **(F)** Histogram showing the averaged proportion of the three
988 different classes of basal contacts. **(G)** Distribution of different types of synapses at the dendrite of

989 B3a bipolar cells. Dendrites (orange) make basal (triangles) contacts. OPL = outer plexiform layer, INL
990 = inner nuclear layer, IPL= inner plexiform layer, PR = Principal member of a double cone, BC =
991 bipolar cell, AC = accessory member of a double cone, G/R = green and red single cones, B/V = blue
992 and violet single cones, TA = triad associated, NTA = non triad associated. Scale bar: G= 5 μ m.

993

994 **Figure 4-5. Characterization of bipolar cell type B3b. (A)** 3D volume reconstruction of complete
995 bipolar cells from this type. Partial bipolar cells that could be assigned to this bipolar cell type are
996 displayed as well. **(B)** Profile sum calculation for B3b bipolar cells (orange) and profile sum of all
997 bipolar cell types (black) in the IPL. **(C)** Dendritic and axonal field mosaics of identified bipolar cell
998 types. **(D)** Correlation between missing branches and number of contacts/bipolar cell indicates, that
999 the number of contacts does not decrease with an increase of missing branches. **(E)** Mean numbers
1000 of ribbon and basal contacts per photoreceptor terminal from each photoreceptor cell type. One way
1001 ANOVA including Tukey test reveals that the most contacted terminal from the principal member of a
1002 double cone has significantly more contacts than the second most contacted terminal. Therefore,
1003 B3b bipolar cells contact predominantly one principal member of a double cone and make less
1004 contacts to other principal members. **(F)** Histogram showing the averaged proportion of the three
1005 different classes of basal contacts. **(G)** Distribution of different types of synapses at the dendrite of
1006 one B3b bipolar cell (** in A). Dendrites (orange) make basal (triangles) contacts. OPL = outer
1007 plexiform layer, INL = inner nuclear layer, IPL= inner plexiform layer, PR = Principal member of a
1008 double cone, BC = bipolar cell, AC = accessory member of a double cone, G/R = green and red single
1009 cones, B/V = blue and violet single cones, TA = triad associated, NTA = non triad associated. Scale bar:
1010 G= 5 μ m.

1011

1012 **Figure 4-6. Characterization of bipolar cell type B4a. (A)** 3D volume reconstruction of complete
1013 bipolar cells from this type. **(B)** Profile sum calculation for B4a bipolar cells (red) and profile sum of all
1014 bipolar cell types (black) in the IPL. **(C)** Dendritic and axonal field mosaics of identified bipolar cell

1015 types. **(D)** Correlation between missing branches and number of contacts/bipolar cell indicates that
1016 the number of contacts does show a higher variation with an increase of missing branches. **(E)** Mean
1017 numbers of ribbon and basal contacts per photoreceptor terminal from each photoreceptor cell type.
1018 Photoreceptor terminals are not significantly different in their number of contacts. **(F)** Histogram
1019 showing the averaged proportion of the three different classes of basal contacts. **(G)** Distribution of
1020 different types of synapses at the dendrite of one B4a bipolar cell. Dendrites (red) make basal
1021 (triangles) contacts. OPL = outer plexiform layer, INL = inner nuclear layer, IPL= inner plexiform layer,
1022 PR = Principal member of a double cone, BC = bipolar cell, AC = accessory member of a double cone,
1023 G/R = green and red single cones, B/V = blue and violet single cones, TA = triad associated, NTA = non
1024 triad associated. Scale bar: G= 5 μ m.

1025
1026 **Figure 4-7. Characterization of bipolar cell type B4b.** **(A)** 3D volume reconstruction of complete
1027 bipolar cells from this type. **(B)** Profile sum calculation for B4b bipolar cells (dark red) and profile sum
1028 of all bipolar cell types (black) in the IPL. **(C)** Dendritic and axonal field mosaics of identified bipolar
1029 cell types. **(D)** Correlation between missing branches and number of contacts/bipolar cell indicates
1030 that the number of contacts does not decrease with an increase of missing branches. **(E)** Mean
1031 numbers of ribbon and basal contacts per photoreceptor terminal from each photoreceptor cell type.
1032 One way ANOVA including Tukey test reveals that the most contacted terminal from the principal
1033 member of a double cone has significantly more contacts than the second most contacted terminal.
1034 Therefore, B4b bipolar cells contact predominantly one principal member of a double cone and make
1035 less contacts to other principal members **(F)** Histogram showing the averaged proportion of the three
1036 different classes of basal contacts. **(G)** Distribution of different types of synapses at the dendrite of
1037 one B4b bipolar cell. Dendrites (dark red) make basal (triangles) contacts. OPL = outer plexiform
1038 layer, INL = inner nuclear layer, IPL= inner plexiform layer, PR = Principal member of a double cone,
1039 BC = bipolar cell, AC = accessory member of a double cone, G/R = green and red single cones, B/V =
1040 blue and violet single cones, TA = triad associated, NTA = non triad associated. Scale bar: G= 5 μ m.

1041

1042 **Figure 4-8. Characterization of bipolar cell type B4c. (A)** 3D volume reconstruction of complete
1043 bipolar cells from this type. Partial bipolar cells that could be assigned to this bipolar cell type are
1044 displayed as well. **(B)** Profile sum calculation for B4c bipolar cells (red) and profile sum of all bipolar
1045 cell types (black) in the IPL. **(C)** Dendritic and axonal field mosaics of identified bipolar cell types. **(D)**
1046 Correlation between missing branches and number of contacts/bipolar cell indicates that the
1047 number of contacts does not decrease with an increase of missing branches. **(E)** Mean numbers of
1048 ribbon and basal contacts per photoreceptor terminal from each photoreceptor cell type. One way
1049 ANOVA including Tukey test reveals that the most contacted terminal from the principal member of a
1050 double cone has significantly more contacts than the second most contacted terminal. Therefore,
1051 B4c bipolar cells contact predominantly one principal member of a double cone and make less
1052 contacts to other principal members **(F)** Histogram showing the averaged proportion of the three
1053 different classes of basal contacts. **(G)** Distribution of different types of synapses at the dendrite of
1054 B4c bipolar cells. Dendrites (red) make basal (triangles) and ribbon (squares) contacts. OPL = outer
1055 plexiform layer, INL = inner nuclear layer, IPL= inner plexiform layer, PR = Principal member of a
1056 double cone, BC = bipolar cell, AC = accessory member of a double cone, G/R = green and red single
1057 cones, B/V = blue and violet single cones, TA = triad associated, NTA = non triad associated. Scale bar:
1058 G= 5 μ m.

1059

1060 **Figure 4-9. Characterization of bipolar cell type B5a. (A)** 3D volume reconstruction of complete
1061 bipolar cells from this type. Partial bipolar cells that could be assigned to this bipolar cell type are
1062 displayed as well. **(B)** Profile sum calculation for B5a bipolar cells (dark orange) and profile sum of all
1063 bipolar cell types (black) in the IPL. **(C)** Dendritic and axonal field mosaics of identified bipolar cell
1064 types **(D)** Correlation between missing branches and number of contacts/bipolar cell indicates that
1065 the number of contacts may decrease with an increase of missing branches. **(E)** Mean numbers of
1066 ribbon and basal contacts per photoreceptor terminal from each photoreceptor cell type. One way

1067 ANOVA including Tukey test reveals that the most contacted terminal from the principal member of a
1068 double cone has significantly more contacts than the second most contacted terminal. Therefore,
1069 B5a bipolar cells contact predominantly one principal member of a double cone and make less
1070 contacts to other principal members. This cell type is a good candidate for a midjet bipolar cell
1071 homolog **(F)** Histogram showing the averaged proportion of the three different classes of basal
1072 contacts. **(G)** Distribution of different types of synapses at the dendrite of B5a bipolar cells. Dendrites
1073 (dark orange) make basal (triangles) and ribbon (squares) contacts. OPL = outer plexiform layer, INL =
1074 inner nuclear layer, IPL= inner plexiform layer, PR = Principal member of a double cone, BC = bipolar
1075 cell, AC = accessory member of a double cone, G/R = green and red single cones, B/V = blue and
1076 violet single cones, TA = triad associated, NTA = non triad associated. Scale bar: G= 5 μ m.

1077

1078 **Figure 4-10. Characterization of bipolar cell type B5b. (A)** 3D volume reconstruction of complete
1079 bipolar cells from this type. **(B)** Profile sum calculation for B5b bipolar cells (yellow) and profile sum
1080 of all bipolar cell types (black) in the IPL. **(C)** Dendritic and axonal field mosaics of identified bipolar
1081 cell types. **(D)** Correlation between missing branches and number of contacts/bipolar cell indicates
1082 that the number of contacts does decrease with an increase of missing branches. **(E)** Mean numbers
1083 of ribbon and basal contacts per photoreceptor terminal from each photoreceptor cell type. Low
1084 number of cells didn't allow further statistical tests. **(F)** Histogram showing the averaged proportion
1085 of the three different classes of basal contacts. **(G)** Distribution of different types of synapses at the
1086 dendrite of a B5b bipolar cell. Dendrites (yellow) make basal (triangles) and ribbon (squares)
1087 contacts. OPL = outer plexiform layer, INL = inner nuclear layer, IPL= inner plexiform layer, PR =
1088 Principal member of a double cone, BC = bipolar cell, AC = accessory member of a double cone, G/R =
1089 green and red single cones, B/V = blue and violet single cones, TA = triad associated, NTA = non triad
1090 associated. Scale bar: G= 5 μ m.

1091

1092 **Figure 4-11. Characterization of bipolar cell type B6. (A)** 3D volume reconstruction of complete
1093 bipolar cells from this type. Partial bipolar cells that could be assigned to this bipolar cell type are
1094 displayed as well. **(B)** Profile sum calculation for B6 bipolar cells (dark orange) and profile sum of all
1095 bipolar cell types (black) in the IPL. **(C)** Dendritic and axonal field mosaics of identified bipolar cell
1096 types. **(D)** Correlation between missing branches and number of contacts/bipolar cell indicates that
1097 the number of contacts does not decrease with an increase of missing branches. **(E)** Mean numbers
1098 of ribbon and basal contacts per photoreceptor terminal from each photoreceptor cell type.
1099 Photoreceptor terminals are not significantly different in their number of contacts. **(F)** Histogram
1100 showing the averaged proportion of the three different classes of basal contacts. **(G)** Distribution of
1101 different types of synapses at the dendrite of a B6 bipolar cell. Dendrites (orange) make basal
1102 (triangles) contacts. OPL = outer plexiform layer, INL = inner nuclear layer, IPL= inner plexiform layer,
1103 PR = Principal member of a double cone, BC = bipolar cell, AC = accessory member of a double cone,
1104 G/R = green and red single cones, B/V = blue and violet single cones, TA = triad associated, NTA = non
1105 triad associated. Scale bar: G= 5 μ m.

1106

1107 **Figure 4-12. Characterization of bipolar cell type B7. (A)** 3D volume reconstruction of complete
1108 bipolar cells from this type. Partial bipolar cells that could be assigned to this bipolar cell type are
1109 displayed as well. **(B)** Profile sum calculation for B7 bipolar cells (light pink) and profile sum of all
1110 bipolar cell types (black) in the IPL. **(C)** Dendritic and axonal field mosaics of identified bipolar cell
1111 types. **(D)** Correlation between missing branches and number of contacts/bipolar cell indicates that
1112 the number of contacts does not decrease with an increase of missing branches. **(E)** Mean numbers
1113 of ribbon and basal contacts per photoreceptor terminal from each photoreceptor cell type.
1114 Photoreceptor terminals are not significantly different in their number of contacts. **(F)** Histogram
1115 showing the averaged proportion of the three different classes of basal contacts. **(G)** Distribution of
1116 different types of synapses at the dendrite of a B7 bipolar cell. Dendrites (light pink) make basal
1117 (triangles) contacts. OPL = outer plexiform layer, INL = inner nuclear layer, IPL= inner plexiform layer,

1118 PR = Principal member of a double cone, BC = bipolar cell, AC = accessory member of a double cone,
1119 G/R = green and red single cones, B/V = blue and violet single cones, TA = triad associated, NTA = non
1120 triad associated. Scale bar: G= 5 μ m.

1121

1122 **Figure 4-13. Characterization of bipolar cell type B8. (A)** 3D volume reconstruction of complete
1123 bipolar cells from this type. Partial bipolar cells that could be assigned to this bipolar cell type are
1124 displayed as well. **(B)** Profile sum calculation for B8 bipolar cells (pink) and profile sum of all bipolar
1125 cell types (black) in the IPL. **(C)** Dendritic and axonal field mosaics of identified bipolar cell types. **(D)**
1126 Correlation between missing branches and number of contacts/bipolar cell indicates that the
1127 number of contacts does not decrease with an increase of missing branches. **(E)** Mean numbers of
1128 ribbon and basal contacts per photoreceptor terminal from each photoreceptor cell type.
1129 Photoreceptor terminals are not significantly different in their number of contacts. **(F)** Histogram
1130 showing the averaged proportion of the three different classes of basal contacts. **(G)** Distribution of
1131 different types of synapses at the dendrite of a B8 bipolar cell. Dendrites (pink) make basal (triangles)
1132 contacts. OPL = outer plexiform layer, INL = inner nuclear layer, IPL= inner plexiform layer, PR =
1133 Principal member of a double cone, BC = bipolar cell, AC = accessory member of a double cone, G/R =
1134 green and red single cones, B/V = blue and violet single cones, TA = triad associated, NTA = non triad
1135 associated. Scale bar: G= 5 μ m.

1136

1137 **Figure 4-14. Characterization of bipolar cell type B9. (A)** 3D volume reconstruction of complete
1138 bipolar cells from this type. Partial bipolar cells that could be assigned to this bipolar cell type are
1139 displayed as well. **(B)** Profile sum calculation for B9 bipolar cells (dark pink) and profile sum of all
1140 bipolar cell types (black) in the IPL. **(C)** Dendritic and axonal field mosaics of identified bipolar cell
1141 types. **(D)** Correlation between missing branches and number of contacts/bipolar cell indicates that
1142 the number of contacts does not decrease with an increase of missing branches. **(E)** Mean numbers
1143 of ribbon and basal contacts per photoreceptor terminal from each photoreceptor cell type.

1144 Photoreceptor terminals are not significantly different in their number of contacts. **(F)** Histogram
1145 showing the averaged proportion of the three different classes of basal contacts. **(G)** Distribution of
1146 different types of synapses at the dendrite of a B9 bipolar cell. Dendrites (dark pink) make basal
1147 (triangles) contacts. OPL = outer plexiform layer, INL = inner nuclear layer, IPL= inner plexiform layer,
1148 PR = Principal member of a double cone, BC = bipolar cell, AC = accessory member of a double cone,
1149 G/R = green and red single cones, B/V = blue and violet single cones, TA = triad associated, NTA = non
1150 triad associated. Scale bar: G= 5 μm .

1151

1152 **Figure 4-15. Characterization of bipolar cell type B10.** **(A)** 3D volume reconstruction of complete
1153 bipolar cells from this type. **(B)** Profile sum calculation for B10 bipolar cells (dark red) and profile sum
1154 of all bipolar cell types (black) in the IPL. **(C)** Dendritic and axonal field mosaics of identified bipolar
1155 cell types. **(D)** Correlation between missing branches and number of contacts/bipolar cell indicates
1156 that the number of contacts does decrease with an increase of missing branches. **(E)** Mean numbers
1157 of ribbon and basal contacts per photoreceptor terminal from each photoreceptor cell type. Not
1158 enough cells to do further analysis **(F)** Histogram showing the averaged proportion of the three
1159 different classes of basal contacts. **(G)** Distribution of different types of synapses at the dendrite of a
1160 B10 bipolar cell. Dendrites (dark red) make basal (triangles) contacts. OPL = outer plexiform layer, INL
1161 = inner nuclear layer, IPL= inner plexiform layer, PR = Principal member of a double cone, BC =
1162 bipolar cell, AC = accessory member of a double cone, G/R = green and red single cones, B/V = blue
1163 and violet single cones, TA = triad associated, NTA = non triad associated. Scale bar: G= 5 μm .

1164

1165 **Figure 4-16. Orphan bipolar cells.** Two bipolar cells which do not map with any of the other types.
1166 Stratification pattern in the IPL is similar but the position of the soma in the INL differs and one cell
1167 contacts all single cone types and the accessory member of the double cone whereas the other cell
1168 only makes one contact to one G/R single cone.

1169

1170 **Figure 4-17. Comparison of bipolar cell types described in different publications. (A)** Identified
1171 bipolar cells in the pigeon retina (Mariani 1987) reorganised to fit our identified bipolar cell types.
1172 We could assign all the identified bipolar cells from Mariani (1987) to our bipolar cells. **(B)** Overview
1173 of our identified bipolar cells from Fig. 4. **(C)** Stratification examples from the chicken retina (adapted
1174 from Yamagata et al. 2021, with permission) showing six out of 22 identified bipolar cells with their
1175 potential stratification in the IPL. We could not find any monostratified cells in our dataset. **(D)**
1176 Identified bipolar cells from the chicken retina (Quesada et al. 1988). Several of the described bipolar
1177 cells look similar to our bipolar cells, however, some of the wide-field bipolar cells are missing in our
1178 dataset.

1179

1180 **Figure 5. Stratification level of the individual bipolar cell types in the OPL and IPL. (A-C)** Bipolar cell
1181 stratification profile in the OPL represented by a probability density function estimate for bipolar cell
1182 types B1a-B3b, B4a-B5b, and B6-B10, respectively. Density functions are calculated based on the
1183 volume of the cells along OPL depth. Dendrites increase in volume with increasing distance to the
1184 connected terminals. Therefore, the OPL density estimate is slightly shifted towards the INL and the
1185 peak density estimate does not represent area of synaptic contacts. **(D-F)** Bipolar cell stratification
1186 profile in the IPL represented by a probability density function estimate for bipolar cell types B1a-
1187 B3b, B4a-B5b, and B6-B10, respectively. OPL = outer plexiform layer, IPL= inner plexiform layer.

1188

1189 **Figure 6. IPL stratification in the chicken retina.** Vertical vibratome sections of the chicken retina
1190 were labelled with PKC (grey; A-D, F, and I), Ctbp2 (magenta; B-C, G-I), GNB3 (green; C, E-F, H-I) and
1191 Dapi (blue; C, F, I). PKC labelled bipolar cell axon terminals are also GNB3 positive in the IPL indicating
1192 that these bipolar cells (high similarity with B9 and B10 in Fig. 4) are ON bipolar cells (D-F). Double
1193 labelling with Ctbp2 and GNB3 reveal ON bipolar axon terminals in the presumed OFF layer and OFF

1194 axon terminals in the presumed ON layer of the IPL (G-J). Complete stack is available in Figure 6-1.

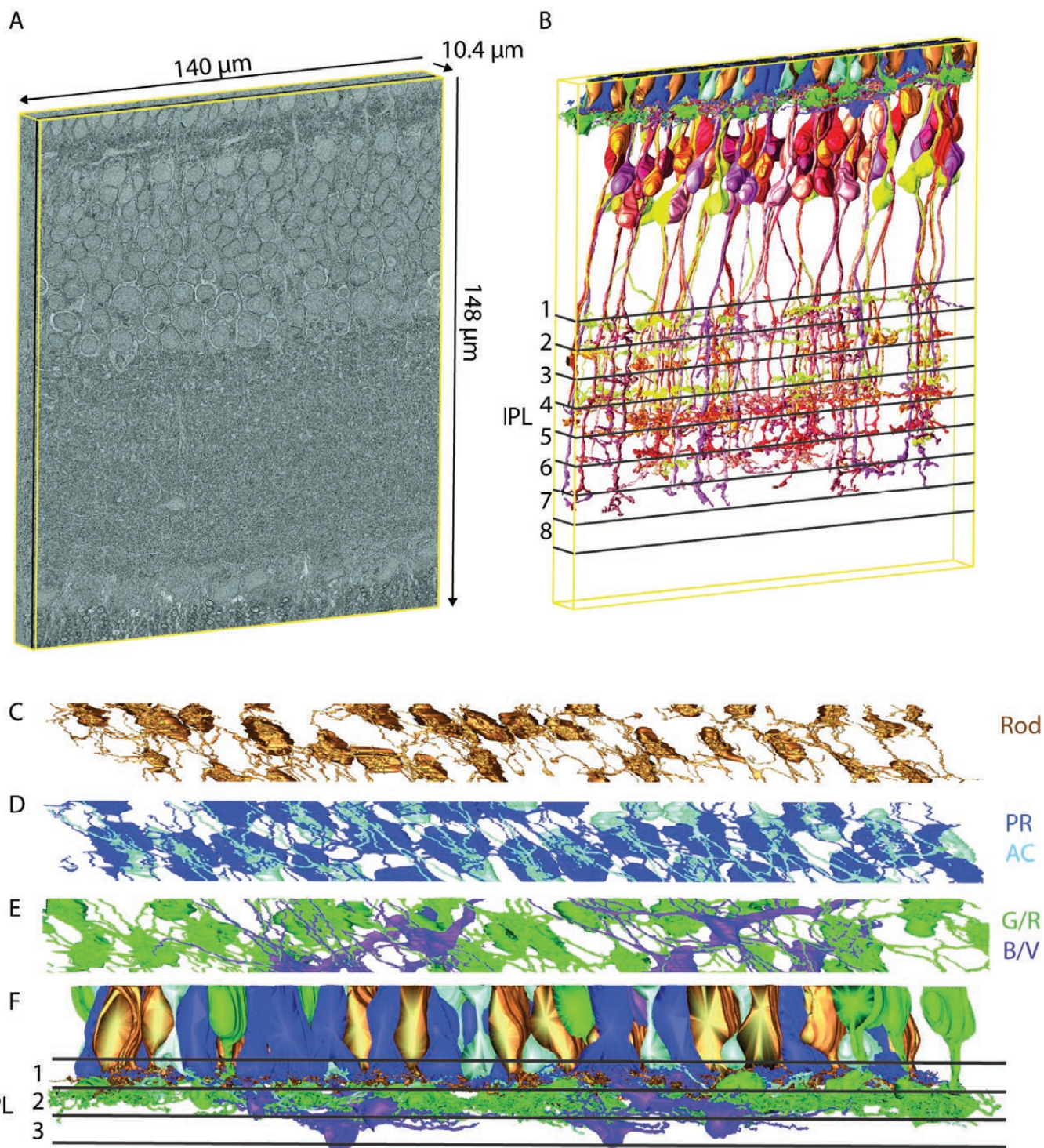
1195 Scale bar in C applies for A-C, scale bar in F for D-J, all scale bars are 20 μm .

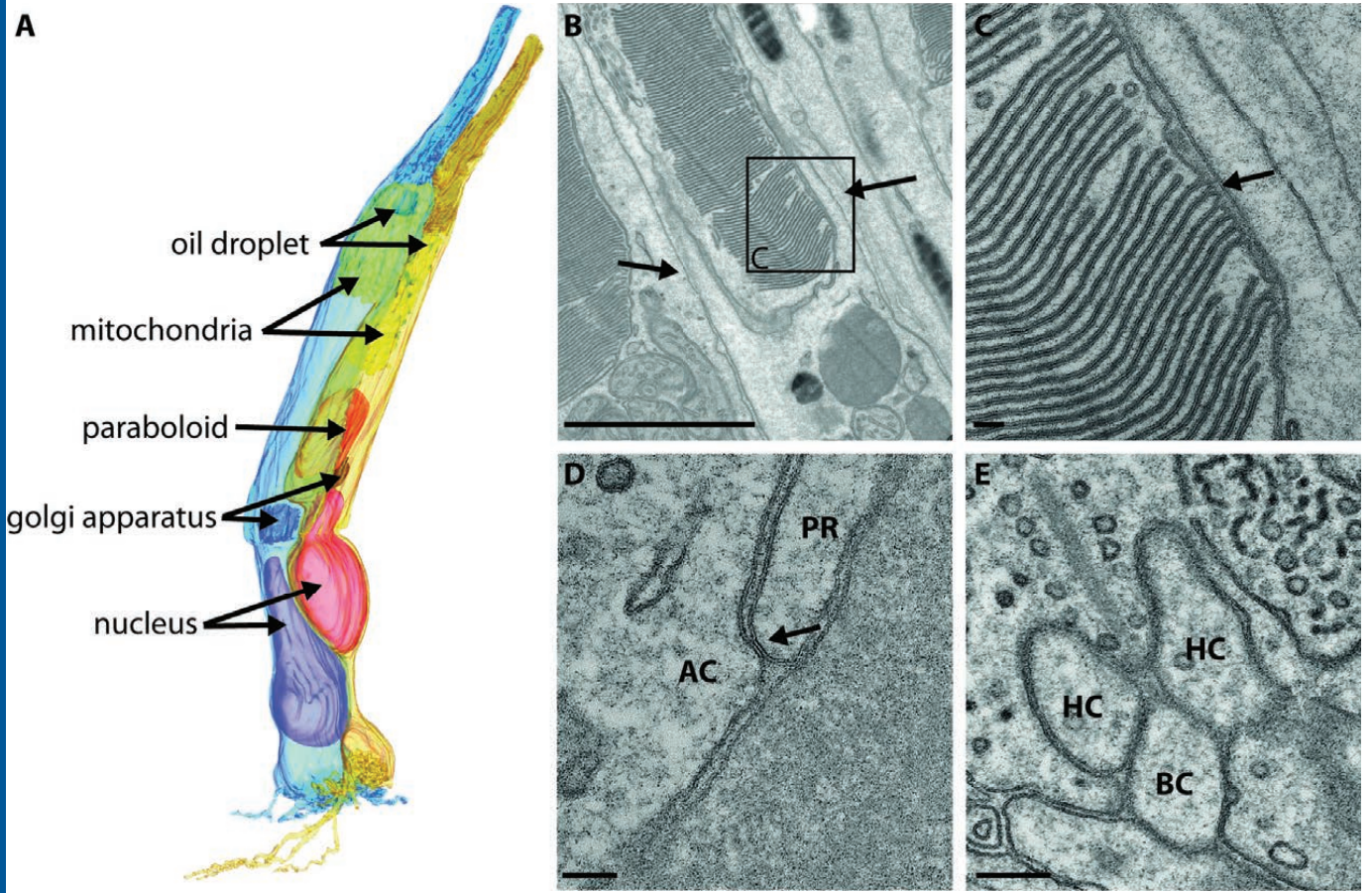
1196

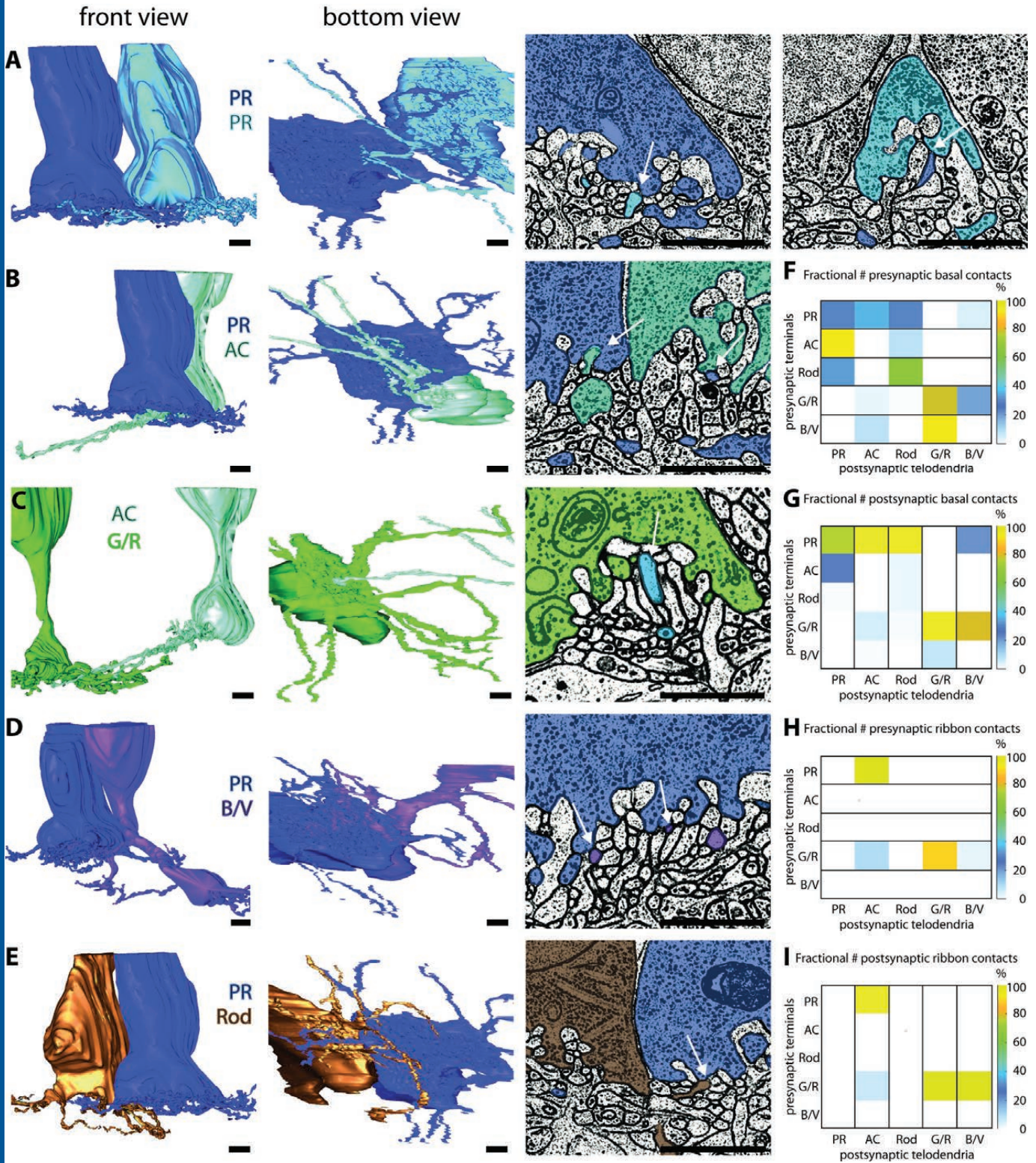
1197 **Figure 6-1 Confocal image stack with GNB3 (green) and Ctbp2 (magenta) staining within the IPL.**

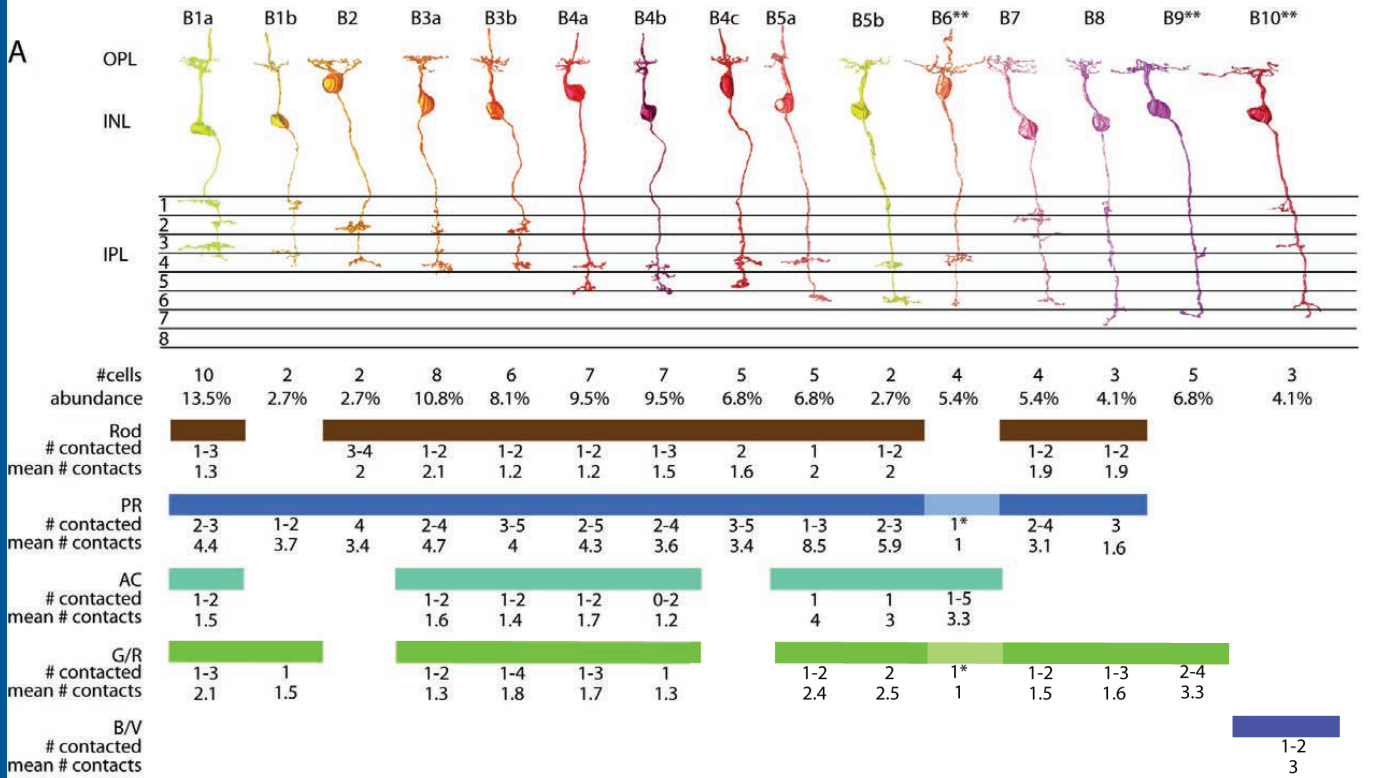
1198

1199









* only one cell of the group made this contact
 ** long unbranched dendrites, a lot reached end of volume

